

Preserving chemical signatures of primordial star formation in the first low-mass stars

Alexander P. Ji^{1*}, Anna Frebel¹ and Volker Bromm²

¹*Kavli Institute for Astrophysics and Space Research and Department of Physics, Massachusetts Institute of Technology, 77 Massachusetts Avenue, Cambridge, MA 02139, USA*

²*Department of Astronomy, University of Texas at Austin, 2511 Speedway, Austin, TX 78712, USA*

Submitted July 2015

ABSTRACT

We model early star forming regions and their chemical enrichment by Population III (Pop III) supernovae with nucleosynthetic yields featuring high [C/Fe] ratios and pair-instability supernova (PISN) signatures. We aim to test how well these chemical abundance signatures are preserved in the gas prior to forming the first long-lived low-mass stars (or second-generation stars). Our results show that second-generation stars can retain the nucleosynthetic signature of their Pop III progenitors, even in the presence of nucleosynthetically normal Pop III core-collapse supernovae. We find that carbon-enhanced metal-poor stars are likely second-generation stars that form in minihaloes. Furthermore, it is likely that the majority of Pop III supernovae produce high [C/Fe] yields. In contrast, metals ejected by a PISN are not concentrated in the first star forming haloes, which may explain the absence of observed PISN signatures in metal-poor stars. We also find that unique Pop III abundance signatures in the gas are quickly wiped out by the emergence of Pop II supernovae. We caution that the observed fractions of stars with Pop III signatures cannot be directly interpreted as the fraction of Pop III stars producing that signature. Such interpretations require modelling the metal enrichment process prior to the second-generation stars' formation, including results from simulations of metal mixing. The full potential of stellar archaeology can likely be reached in ultra-faint dwarf galaxies, where the simple formation history may allow for straightforward identification of second-generation stars.

Key words: dark ages, reionization, first stars – stars: Population II – stars: Population III – stars: chemically peculiar – galaxies: high-redshift – galaxies: formation

1 INTRODUCTION

The formation of the first, so-called Population III (Pop III), stars marks an important yet incompletely understood period in cosmic history. As the first non-linear baryonic structures in the Universe, Pop III stars initiate the reionization and chemical enrichment of the early intergalactic medium, thus setting the stage for the assembly of more mature galaxies (e.g. Bromm et al. 2009; Loeb & Furlanetto 2013, and references therein).

The character of Pop III star formation has been theoretically investigated in great detail, and simulations of this process have begun to converge on consistent conclusions (Bromm 2013; Glover 2013; Greif 2015). Unfortunately, observations that can directly constrain these ideas are in short supply. The James Webb Space Telescope (JWST) may be able to observe supernovae (SNe) from the most massive

Pop III stars (Hummel et al. 2012; Pan et al. 2012; Whalen et al. 2013; Chen et al. 2014; de Souza et al. 2014). The lack of observed low-mass Pop III stars in the Milky Way can potentially constrain the low end of the Pop III initial mass function (IMF), a constraint that will gain in strength with increasing survey sizes (Hartwig et al. 2015). The ionizing effect of Pop III stars may be seen in epoch of reionization measurements (Greif & Bromm 2006), although this prospect has significantly weakened in light of the recent *Planck* determination of a lower optical depth to Thomson scattering (Planck Collaboration et al. 2015). Arguably, in the absence of such direct probes, the best available constraints on Pop III star formation may come from chemical abundances in the most metal-poor stars, which preserve the chemical composition of their birth clouds in their stellar atmospheres (e.g. Karlsson et al. 2013; Frebel & Norris 2015). The ideal objects for probing Pop III star formation are the first metal-enriched low-mass stars (or *second-generation stars*), which contain only metals from Pop III stars.

* E-mail: alexji@mit.edu

It is not known with any certainty what abundance signatures would clearly indicate enrichment primarily by Pop III stars, but intriguing empirical hints have been found. Some unique abundance patterns have been identified in metal-poor stars, including the high fraction of carbon-enhanced metal-poor (CEMP) stars at extremely low iron abundance (e.g. Norris et al. 2013; Placco et al. 2014), and a strong odd-even effect characteristic of pair-instability supernovae (PISNe) (Heger & Woosley 2002; Aoki et al. 2014). However, average metal-poor halo stellar abundances ($[\text{Fe}/\text{H}] < -2.5$) suggest that the majority of Pop III stars died as core-collapse supernovae (CCSNe) (Joggerst et al. 2010). As the ejecta from multiple SNe mix together, any unique Pop III abundance patterns which could be preserved in metal-poor stars will be diluted away to an average core collapse SN yield.

Recent simulations have suggested that second-generation stars should generically form by combining the metal yields from more than one Pop III SN explosion, even in the simplest sites of second generation star formation (Ritter et al. 2015; Jeon et al. 2015). Such an immediate enrichment by multiple SNe could rapidly dilute away unique Pop III chemical signatures in the majority of the subsequent, Pop II, star formation events. Modeling such dilution from multiple SNe is a classical problem in the theory of chemical evolution. Several approaches have been employed, including models that assume instantaneous mixing (e.g. Tinsley 1980; Kirby et al. 2011), extensions that allow inhomogeneous mixing (e.g. Oey 2000; Argast et al. 2004; Karlsson 2005), and full hydrodynamic simulations (e.g. Kobayashi & Nakasato 2011; Webster et al. 2014). These models were all devised to study chemical evolution in a static self-enriching system over multiple generations, such as the Milky Way disc or a large dwarf galaxy, with the exception of Webster et al. 2014 who specifically investigate chemical evolution in ultra-faint dwarf galaxies. However, second-generation stars form in a unique initial stage of chemical enrichment, taking place in the earliest, low-mass building blocks of galaxy formation. The existing chemical evolution models focus less on the initial chemical enrichment stage and more on the subsequent chemical evolution.

In this paper, we investigate how mixing the ejecta from multiple SNe may remove tell-tale nucleosynthetic signatures from Pop III stars. We consider second-generation star formation in the simplest possible environments motivated by cosmological simulations of the early Universe. Considering these environments, we apply idealized mixing models to predict when the Pop III signature is preserved by metal-poor stars and can be probed by stellar archaeology.

The structure of our paper is as follows. In Section 2, we discuss what is known about where and how stars form in the early Universe. In Section 3, we describe mixing models to produce chemical distributions both for second-generation stars and subsequent generations of stars. The results of our models are presented in Section 4, and we conclude in Section 5. Whenever needed, we use a cosmology with parameters $\Omega_m = 0.3$, $\Omega_\Lambda = 0.7$, $h = 0.7$, and $\Omega_b = 0.05$. The baryon fraction then is $f_b = 1/6$. When gas is ionized and neutral, we use $\mu_{\text{ionized}} = 0.59$ and $\mu_{\text{neutral}} = 1.23$, respectively, where μm_p is the mean molecular weight of the gas.

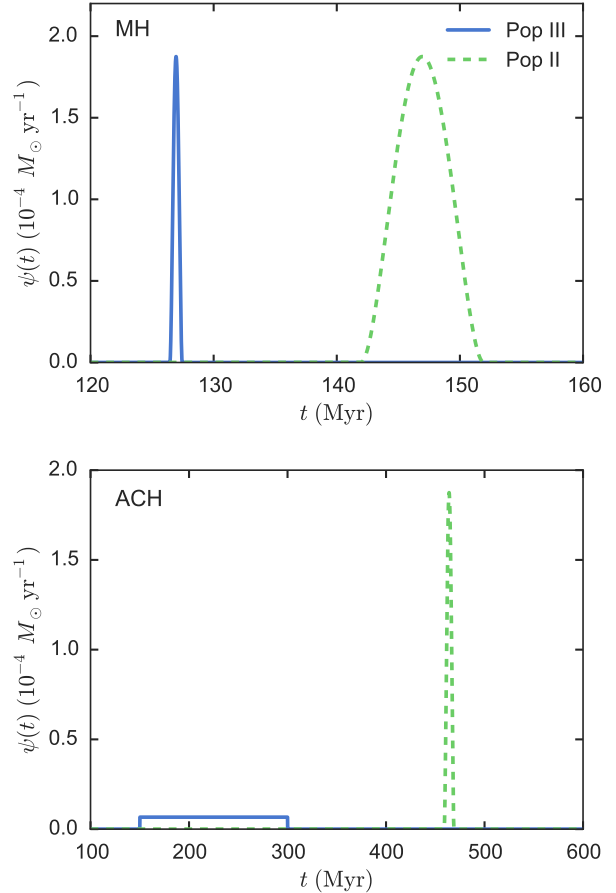


Figure 1. Schematic early star formation rates. Top: minihalo star formation rates. Pop III forms $100M_\odot$ in a 10^5 yr burst at virialization ($z = 25$). Pop II forms $1000M_\odot$ in a 10 Myr burst after a recovery time of 20 Myr. Bottom: atomic cooling halo star formation rates. Pop III forms $1000M_\odot$ uniformly over 150 Myr following the merger tree in Greif et al. (2008). A Pop II burst at virialization ($z = 10$) forms $1000M_\odot$ of stars over 10 Myr.

2 STAR FORMATION IN THE EARLY UNIVERSE

To model the first chemical enrichment events, we must consider the nature of star formation in the early Universe. Here, we take an ab initio approach to understanding early star formation based on theoretical arguments and review the insights obtained from simulations. The picture described here motivates the mixing models presented in Section 3.

Structure formation in Λ CDM is a hierarchical process, with small dark matter haloes forming early and merging into larger haloes. Two environments stand out in the early Universe where first star formation can take place. These environments correspond to the two most significant cooling mechanisms in metal-poor gas. The first stars in the Universe form in minihaloes, where star formation is triggered by molecular hydrogen cooling (e.g. Tegmark et al. 1997). The first galaxies in the Universe likely form in atomic cooling haloes, when hydrogen line cooling becomes significant (e.g. Oh & Haiman 2002). Cosmological simulations of these two environments have outlined a general picture for the for-

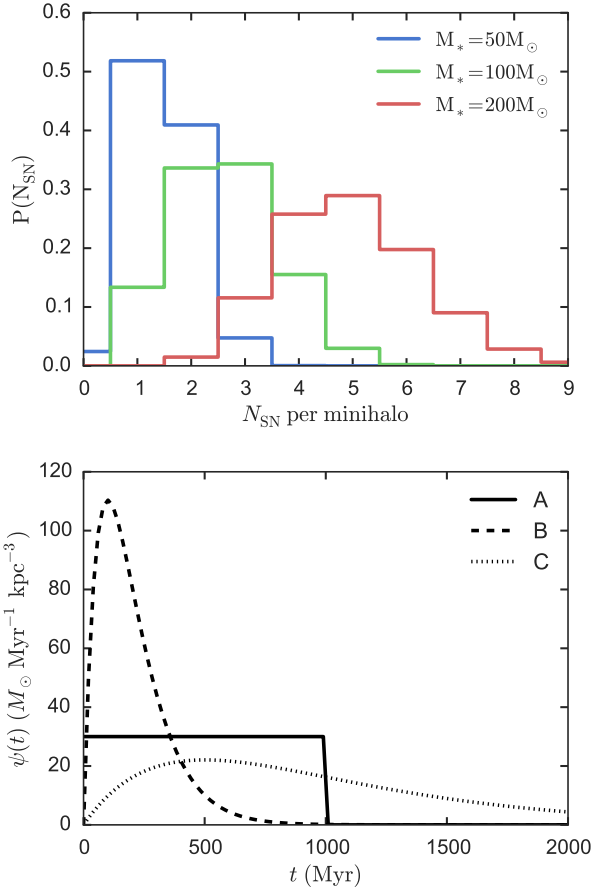


Figure 2. Top: distribution of number of Pop III SNe per minihalo, assuming $100M_{\odot}$ of Pop III stars form. This was computed as described in the text from 10^6 minihaloes, assuming stars with $M \geq 10M_{\odot}$ turn into SNe. Bottom: Pop II star formation rates for a self-enriching atomic cooling halo. Model A is a 1 Gyr flat star formation rate. Model B is a 100 Myr burst. Model C is a 500 Myr burst.

mation of Pop III stars and the first few generations of Pop II stars, which we describe in Sections 2.1 and 2.2. The star formation rates described are shown schematically in Figure 1. We discuss nucleosynthetic signatures from the first generations of stars in Section 2.3.

2.1 Population III star formation

2.1.1 Pop III initial mass function

Pop III stars form in minihaloes of mass $\sim 10^6 M_{\odot}$ around $z \sim 25$, where star formation is triggered by molecular hydrogen cooling (Couchman & Rees 1986; Haiman et al. 1996; Tegmark et al. 1997). The lack of metal cooling and the resulting higher temperatures suggest that Pop III stars have high characteristic masses, but our understanding of the characteristic mass has changed considerably over the last decade (e.g. Bromm 2013). Early simulations found that these stars might have characteristic masses $\gtrsim 100M_{\odot}$ with one star forming per minihalo (Abel et al. 2002; Bromm et al. 2002; Yoshida et al. 2006; O’Shea & Norman 2007). These stars would typically explode as PISNe with explo-

sion energies $\gtrsim 10^{52}$ erg (e.g. Heger & Woosley 2002). The strong feedback from these stars likely prevents further star formation within their host minihaloes (Greif et al. 2007; Whalen et al. 2008).

However, more recent studies with higher spatial resolution have found that fragmentation may occur in the disc surrounding a Pop III protostar, forming small multiples of stars with lower characteristic masses $\gtrsim 10M_{\odot}$ (Clark et al. 2008, 2011; Stacy et al. 2010; Greif et al. 2011, 2012). The amount of fragmentation varies between different minihaloes and depends on the detailed thermal history of the gas (Greif et al. 2012). This general picture has been corroborated by observations of metal-poor stars, which seem to show clear α -element enhancements that are consistent with core-collapse supernovae (e.g. Beers & Christlieb 2005).

Although a shape and range of the IMF cannot yet be determined robustly, Greif et al. (2011) find that the protostellar mass function across five minihaloes is approximately logarithmically flat ranging from $\sim 0.1 - 10M_{\odot}$ based on 1000 years of fragmentation and accretion, although accretion should continue for 10^5 or 10^6 years in total. Susa et al. (2014) evolve 59 minihaloes with lower resolution for $\sim 10^5$ years after sink particle formation, also finding a fairly logarithmically flat IMF ranging from $\sim 1 - 100M_{\odot}$. Such simulations suggest that the Pop III IMF is close to logarithmically flat from $\sim 1 - 100M_{\odot}$ (with a characteristic mass $\sim 20M_{\odot}$), though a flat IMF is also reasonable (e.g. Cooke & Madau 2014)¹. With such an IMF, it is likely that multiple CCSNe form within each minihalo. Thus, we use a log-flat IMF with lower and upper mass bounds of 1 and $100M_{\odot}$.

The mass range suggested here does not allow for higher mass PISNe. If PISNe occur, the PISN progenitor is likely the only Pop III star to form in a given minihalo. There is currently only tentative evidence for metal-poor stars with PISN abundance patterns (Aoki et al. 2014), because PISN signatures may only be found in higher metallicity stars and thus be missed by current metal-poor star surveys which preferentially select the most metal-poor stars (Karlsson et al. 2008). In addition, superluminous supernovae which might be associated with PISNe have been observed at both high and low redshift (Gal-Yam et al. 2009; Cooke et al. 2012). If a PISN explodes in a minihalo, the violent feedback associated with it will likely prevent any subsequent star formation there.

2.1.2 Pop III star formation rate

The Pop III star formation in an individual minihalo should occur in one burst. Collapse begins around the virialization time of the dark matter halo, and stars form in about a free fall time. The mass accretion rates into the central star forming regions are around $10^{-3} - 10^{-2} M_{\odot} \text{ yr}^{-1}$ for $\sim 10^5$ yr (e.g. Greif et al. 2011; Hirano et al. 2014; Susa et al. 2014). Not all of this mass ends up in protostars due to radiation feedback (Stacy et al. 2012), and each minihalo ends up forming around $100M_{\odot}$ of stars (e.g. Susa et al. 2014).

Although our Pop III IMF allows low mass stars to form, for the investigation of metal enrichment we are only

¹ A logarithmically flat IMF has $dN/d\log M \propto \text{constant}$, while a flat IMF has $dN/dM \propto \text{constant}$.

interested in high mass stars which explode as SNe. The exact number of SNe in a minihalo is not well determined; simulations which resolve significant fragmentation do not run long enough to determine the actual stellar masses (e.g. Greif et al. 2011), while simulations running for longer times may not fully resolve the fragmentation (e.g. Hirano et al. 2014; Susa et al. 2014). As a simple way to model the number of Pop III SNe exploding within a minihalo, we sequentially draw stellar masses from the log-flat IMF ranging over $1 - 100M_{\odot}$ until we reach a total of $M_{*} = 50, 100, \text{ or } 200M_{\odot}$ of stars. If adding a star would cause us to increase the mass beyond M_{*} , we redraw from the IMF. Only stars with mass larger than $10M_{\odot}$ are assumed to undergo a supernova, so we stop when we have drawn $> M_{*} - 10M_{\odot}$ of stars. The distribution of the number of SNe found this way from 10^6 minihaloes is shown in Figure 2.

This procedure gives initial stellar masses in addition to the total number of SNe in a minihalo, and in principle the stellar masses can be used as inputs to SNe nucleosynthesis calculations to determine the metal yields on a star-by-star basis. However, given the uncertainties in these calculations (see Section 2.3), we aim to separate the impact of SN yields and energies from the problem of metal mixing. Thus, we do not use the stellar masses derived from this procedure for anything other than estimating the number of SNe in a minihalo.

Pop III stars will not form in atomic cooling haloes, unless in rare cases, because the haloes will typically be polluted with metals prior to their virialization (e.g. Johnson et al. 2008). One can instead estimate the number of star forming minihaloes that eventually merge into an atomic cooling halo. Greif et al. (2008) followed one atomic cooling halo and found that the ejecta from ~ 10 star forming minihaloes mixed together during the formation of the atomic cooling halo, with the Pop III star formation occurring from $t = 150 - 300 \text{ Myr}$. If each minihalo produces $\sim 100M_{\odot}$ of Pop III stars, the Pop III star formation rate is about $1000M_{\odot}$ in 150 Myr . For an extreme upper bound, a maximum of one hundred 10^6M_{\odot} minihaloes can make up a single 10^8M_{\odot} atomic cooling halo.

2.2 Population II star formation

In this section we describe the formation of Pop II stars. The transition from Pop III to Pop II is often demarcated by a critical metallicity. The critical metallicity could be set by atomic line cooling (e.g. Bromm & Loeb 2003; Frebel et al. 2007) or dust thermal cooling (e.g. Schneider et al. 2012; Ji et al. 2014). For simplicity, we do not apply any critical metallicity, and instead assume all metal-enriched gas is able to form low mass Pop II stars that could correspond to metal-poor stars. In practice, our modelled metallicities are nearly always above $Z \sim 10^{-5}Z_{\odot}$, which places all gas above the critical metallicity for low-mass star formation according to the dust cooling criterion.

2.2.1 Pop II star formation environment

Both the minihalo and atomic cooling halo environments may host early Pop II star formation. Which environment is relevant in a given region of space depends on the degree of

Table 1. Second-generation star forming environments

	Minihalo	Atomic Cooling Halo
Halo Mass	10^6M_{\odot}	10^8M_{\odot}
z_{vir}	25	10
R_{vir}	120 pc	1.3 kpc
v_{vir}	6 km s^{-1}	18 km s^{-1}
T_{vir}	1900 K	17400 K
D_t^a [$\text{kpc}^2 \text{ Myr}^{-1}$]	2.4×10^{-5}	8.1×10^{-4}

^a effective diffusion coefficient for turbulent mixing

Pop III feedback and the corresponding recovery time (Jeon et al. 2014).

If Pop III feedback is strong, then the minihalo loses most of its gas (e.g. Whalen et al. 2008) and the next time gas can collapse is in atomic cooling haloes with virial temperature $\sim 10^4 \text{ K}$ or mass $\sim 10^8M_{\odot}$ (Oh & Haiman 2002; Greif et al. 2008; Wise et al. 2012). These haloes are perhaps the best candidates for sites of first galaxies (Bromm & Yoshida 2011). If instead Pop III feedback is weak, then it is possible for gas to recollapse in the original minihalo and form Pop II stars there (e.g. Ritter et al. 2012, 2015; Cooke & Madau 2014). These stars form out of a mix between the supernova ejecta that have fallen back and primordial gas inflowing to the centre of the minihalo through filaments. The minihalo may gain some mass during the recollapse (Jeon et al. 2014).

It is likely that differing accretion/merger histories and the distribution of Pop III stellar masses result in different recovery times, allowing second-generation stars to form from both of these environments. The atomic cooling halo and minihalo will be the two main contributors to the population of second-generation stars in the Λ CDM paradigm. However, there are two other situations that may arise. It is possible that the blast from a PISN in one minihalo is able to pollute a nearby minihalo and trigger second-generation star formation (e.g. Greif et al. 2010; Wise et al. 2012; Smith et al. 2015), although the degree of metal pollution may not be very high (Cen & Riquelme 2008). Also, star formation may be triggered in the shocked shell of a Pop III supernova explosion (e.g. Mackey et al. 2003; Chiaki et al. 2013). These two cases are possible variants on the picture of metal recollapse in a minihalo which depend on the specific hydrodynamics of metal mixing and supernova shocks, and we do not expect the majority of second-generation stars to form through such mechanisms. However, such cases may be able to sample the metal output of individual SNe.

As canonical values, we consider minihaloes of mass $\sim 10^6M_{\odot}$ virializing at $z \sim 25$, and in case of moderate stellar feedback we assume second-generation (Pop II) star formation takes place in a similar environment. For the atomic cooling halo case, we assume a typical halo mass of $\sim 10^8M_{\odot}$, virializing at $z \sim 10$ (Greif et al. 2008). Note that in both these environments, there will be a distribution of halo masses and virialization redshifts (Wise et al. 2012; Hirano et al. 2014; Susa et al. 2014). The halo mass is especially important in the minihalo case as a higher halo mass increases the likelihood that second-generation stars can form within the minihalo (Cooke & Madau 2014; Jeon et al. 2014). Canonical physical parameters of these haloes are given in Table 1.

Regardless of whether a second-generation star forms in a minihalo or an atomic cooling halo, it is very likely that metals from multiple Pop III SN will contribute to the second-generation star forming gas, for the following reasons. If the second-generation star forms in an atomic cooling halo, its metal content is determined by mixing together metals from many progenitor minihaloes. If instead the second-generation star forms in a minihalo, the Pop III stars which formed in that minihalo were of lower mass, resulting in less vigorous feedback. Thus, it is likely that a small multiple of Pop III stars contributed metals to second-generation stars.

2.2.2 Pop II star formation rates

When Pop II star formation occurs in a minihalo, the SN ejecta are mixed with pristine infalling gas, accreting through filaments, in a turbulent core, collapsing after a recovery time of ~ 20 Myr (Jeon et al. 2014; Ritter et al. 2015). The rate of Pop II star formation in this case has not been simulated, but in the study by Ritter et al. (2012) the cool dense gas core at the centre has a mass $\sim 3000M_{\odot}$. If the star formation efficiency is ~ 30 per cent, then this will ultimately produce $\sim 1000M_{\odot}$ of stars in ~ 10 Myr. After 10 Myr, the more massive Pop II stars will explode as supernovae (~ 5 SNe). If a sufficient number of SNe explode and the minihalo is not too massive, this will finish the gas expulsion initiated by the Pop III stars and halt star formation in the minihalo until it merges into another system. On the other hand, if the minihalo has gained enough mass to contain the SN explosion, then the minihalo can continue to self-enrich and form stars out of gas contaminated by Pop II SNe (Jeon et al. 2014).

Pop II star formation in an atomic cooling halo begins approximately when the halo virializes ($z \sim 10$ or $t \sim 400$ Myr) and atomic line cooling triggers star formation (e.g. Greif et al. 2008; Safranek-Shrader et al. 2014b,a). The first burst of star formation will occur near the centre of the atomic cooling halo, after which star formation will be temporarily halted. Stars forming after this initial ~ 10 Myr burst of Pop II star formation will no longer be truly second-generation stars, having been polluted by the first generation of Pop II stars. The amount of stars formed in this burst is not certain. Greif et al. (2008) find that $10^5 M_{\odot}$ of cold dense gas has collapsed with $Z \sim 10^{-3} Z_{\odot}$. Safranek-Shrader et al. (2014a) follow collapse to a gas density of 10^7 cm^{-3} and find that stellar clusters can form with $\sim 1000M_{\odot}$ of stars after 4 Myr. Safranek-Shrader et al. (2015) resolve the same initial conditions down to a density of $\sim 10^{13} \text{ cm}^{-3}$, resolving individual protostellar cores as sink particles and including the effect of their radiative feedback. In 20,000 yr, $\sim 80M_{\odot}$ of stars formed, although many of the protostars will continue to accrete gas beyond the simulated time. Thus it appears that approximately $1000M_{\odot}$ of second-generation stars can form in this initial 10 Myr burst. The SNe from this burst likely contaminate the dense gas with metals from Pop II stars (Wada & Venkatesan 2003), preventing further second-generation stars from forming afterwards.

After the initial burst, Pop II star formation in the atomic cooling halo will continue until it is halted. This could happen externally through reionization or merging into another halo, or it could happen internally through SN

Table 2. CEMP signature supernova yields

	CCSN ^a	Faint SN ^b	Wind+SN ^c	Pop II SN ^d
Mass (M_{\odot})	20	20	20	20
$E_{\text{SN},51}$ ^e	1	0.74	1	1
C (M_{\odot})	0.211	0.20	1.034	0.128
Fe (M_{\odot})	0.072	1.09×10^{-5}	0.072	0.073

^a Nomoto et al. 2006

^b Iwamoto et al. 2005

^c CCSN with added C from Hirschi 2007 (see text)

^d Nomoto et al. 2013

^e $E_{\text{SN},51}$ is the explosion energy in units of 10^{51} erg

feedback. We estimate these processes with three models. Model A is a constant star formation rate for 1 Gyr followed by an abrupt cutoff. Model B is a short ~ 100 Myr burst. Model C is a longer ~ 500 Myr burst. The burst in models B and C use the equation

$$\psi(t) = \psi_0 \left(\frac{t}{\tau} \right) e^{-t/\tau} \quad (1)$$

where ψ_0 is some normalization and τ is the characteristic time of the burst (100 Myr and 500 Myr for models B and C, respectively). These star formation rates are plotted in Figure 2. The normalizations are all set to produce $30,000 M_{\odot} \text{ kpc}^{-3}$.

2.2.3 Pop II initial mass function

Modern star formation theory has recognized the importance of supersonic turbulence in regulating star formation (Mac Low & Klessen 2004; McKee & Ostriker 2007). The turbulent velocity helps prevent global gravitational collapse, while the complex network of shocks formed by supersonic flows create local density fluctuations that can trigger star formation. The turbulent density spectrum may play a fundamental role in determining the IMF (Hopkins 2012).

In atomic cooling haloes, supersonic turbulence is created during virialization of the halo, and during subsequent accretion from the cosmic web (e.g. Greif et al. 2008; Safranek-Shrader et al. 2014a,b). This suggests that the Pop II IMF in atomic cooling haloes may be similar to that in present-day star formation. We thus take the IMF in atomic cooling haloes to be the Salpeter IMF from $0.1 - 100 M_{\odot}$. To date, there have not been significant studies of turbulence in minihaloes which have experienced recollapsing gas. We assume the IMF in this situation is also Salpeter.

2.3 Nucleosynthetic signatures

We now discuss the Pop III chemical abundance signatures that may be found in second-generation stars, as well as other early metal sources. Unfortunately, calculating supernovae yields from first principles is a difficult task. Core collapse supernovae in particular have proven to be difficult to understand from first principles due to a complex explosion mechanism. After the star's core becomes gravitationally unstable and undergoes core bounce, the outgoing shock stalls and is presumably revived by some combination of hydrodynamic instabilities and neutrino heating (e.g. Janka et al.

Table 3. PISN signature supernova yields

	CCSN ^a	PISN ^b	Pop II SN ^c
Prog. Mass (M_{\odot})	20	195	20
$E_{\text{SN},51}$	1	40	1
C (M_{\odot})	0.211	4.13	0.128
Na (M_{\odot})	0.0029	0.00028	0.00181
Mg (M_{\odot})	0.150	4.39	0.247
Ca (M_{\odot})	0.00623	0.993	0.00921
Fe (M_{\odot})	0.072	3.08	0.073
Co (M_{\odot})	1.5×10^{-4}	5.59×10^{-6}	6.21×10^{-5}
Ni (M_{\odot})	0.00175	0.00825	7.11×10^{-4}

^a Nomoto et al. 2006^b Heger & Woosley 2002^c Nomoto et al. 2013

2012). 3D simulations of SN explosions that treat multifrequency neutrino transport are a recent development, and the results of these calculations have not yet converged between different groups (e.g. Hanke et al. 2013; Mezzacappa et al. 2014). Instead of a full hydrodynamic simulation, CCSN metal yield calculations often parametrize the explosion in different ways (e.g. Kobayashi et al. 2006; Heger & Woosley 2010; Limongi & Chieffi 2012). These methods agree qualitatively, but not in detail (Nomoto et al. 2013).

Rather than looking to reproduce detailed elemental abundances, we instead focus on the most important broad signatures of Pop III nucleosynthesis. Many Pop III CCSN calculations tend to produce abundances consistent with the stellar halo chemical record (e.g. Tumlinson 2006; Joggerst et al. 2010), suggesting that Pop III CCSNe produce a standard α -enhanced yield not qualitatively different from their higher metallicity counterparts. As a representative yield, we take the $20M_{\odot}$, zero-metallicity model with a SN explosion energy of $E_{\text{SN}} = 10^{51}$ erg from Nomoto et al. (2006).

However, there are two abundance signatures that may distinguish themselves from this typical yield pattern, the carbon enhanced metal-poor (CEMP) signature and the pair instability supernova (PISN) signature. We now discuss these signatures in more detail.

The exact yields we use in our future models are given in Tables 2 and 3. We have quoted the yields with a high degree of precision, but the yields will likely span a range of values. Our adopted values are only meant to be representative realizations.

2.3.1 CEMP signature

If a star has $[\text{C}/\text{Fe}] > 0.7$, we say it displays the *CEMP signature* following Aoki et al. (2007)². It is not known whether the CEMP signature is created by Pop III stars, or if there is a non-primordial explanation related to surface pollution or a critical metallicity (see Norris et al. 2013, and Nomoto et al. 2013, for a comprehensive account of possibilities, and Sluder et al. 2015 for a mechanism not previously considered). We proceed under the assumption the CEMP signature does indeed trace nucleosynthetic yields of Pop III stars. There are two classes of mechanisms to create the signature.

It can be produced either by removing iron from or adding carbon to the standard CCSN yields.

A likely mechanism for removing iron is to allow some sort of metal fallback during the SN explosion. This can be accomplished through faint supernovae that undergo mixing and fallback (Umeda & Nomoto 2002, 2003; Iwamoto et al. 2005) or a jet-like explosion (Tominaga et al. 2007). As a representative fallback yield, we take a faint CCSN with $E_{\text{SN}} = 0.74 \times 10^{51}$ erg from Iwamoto et al. (2005) which reproduces the detailed abundances of HE 1327–2326 (Frebel et al. 2005).

A likely mechanism for adding carbon to the yield is by winds from rotating massive Pop III stars (Meynet et al. 2006, 2010; Hirschi 2007). To approximate this, we add $0.823M_{\odot}$ of carbon to our standard Pop III CCSN. This represents the carbon winds from a very fast rotating star of $20M_{\odot}$ (Hirschi 2007), and results in $[\text{C}/\text{Fe}] = 0.89$ for the wind model.

2.3.2 PISN signature

The PISN signature is still a theoretical signature, although it has been tentatively observed in a metal-poor star (Aoki et al. 2014). In contrast with CCSNe, the explosion mechanism for PISNe is better understood and does not need to be put in artificially (e.g. Heger & Woosley 2002). The typical PISN turns a large fraction of its stellar mass into metals and exhibits suppressed odd-even abundance ratios. We will consider a star to have the PISN signature if $[\text{Co}/\text{Ni}] < -0.5$, where Co and Ni are representative odd and even elements. We take the yields from Heger & Woosley (2002) for a $195M_{\odot}$ $E_{\text{SN}} \sim 40 \times 10^{51}$ erg explosion as a characteristic PISN yield.

2.3.3 Other metal sources

It will be of interest to look at how Pop II SNe dilute away the CEMP and PISN abundance signatures. For Pop II SN yields, we use the $20M_{\odot}$, $Z = 0.001$ yields from Nomoto et al. (2013) which are similar to the Pop III CCSNe yields.

There are two other main sources of metals in standard chemical evolution models: AGB stars and Type Ia SNe. Low-to-intermediate mass stars undergo an AGB phase, during which they expel significant amounts of carbon in their winds. A typical time until an intermediate-mass star undergoes the AGB phase is ~ 100 Myr, much longer than the recovery time if second-generation stars form in minihaloes, but shorter than the recovery time for an atomic cooling halo. However, the total metal mass from a single AGB star's winds is not very large, and its importance in standard chemical evolution is largely due to the steep slope of the IMF. The top-heavy Pop III IMF suggests that AGB stars will not be an important contributor to elements found in second-generation stars. Type Ia SNe produce large amounts of iron-peak elements. In principle, there could be Pop III binary white dwarfs that produce Type Ias. These also are unlikely to contribute to second-generation stars, since such systems may be rare, and the delay time between their formation and detonation is typically ~ 1 Gyr (although it could be as low as 100 Myr, see Maoz et al. 2012). For these reasons, we will not consider contributions from these two metal sources.

² $[\text{X}/\text{Y}] = \log_{10}(N_{\text{X}}/N_{\text{Y}}) - \log_{10}(N_{\text{X}}/N_{\text{Y}})_{\odot}$ for element X, Y

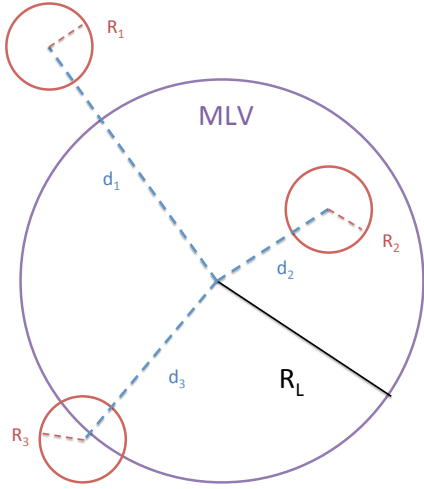


Figure 3. Illustrating the enrichment model for an atomic cooling halo (Section 3.2). The Mixed Lagrangian Volume (MLV) has a Lagrangian radius $R_L = 6.4$ kpc at $z = 10$. Not shown is the size of the ACH Lagrangian Volume (ALV), which has a radius $R_{L,ACH} = 11.4$ kpc at $z = 10$. Here, three minihaloes have experienced SN explosions. In this example, $q_1 = 0$, $q_2 = 1$, and q_3 is between 0 and 1. The distances d_i are uniformly drawn from a spherical volume \mathcal{V} (not shown) whose radius is larger than $R_L + \max\{R_i\}$.

3 METAL ENRICHMENT MODELS

As seen in Section 2, most second-generation stars form out of gas that has been enriched by multiple SNe, even in the simplest possible environments of minihaloes (MH) and atomic cooling haloes (ACH). Thus, there are two fundamental questions we must answer to understand when a unique Pop III chemical abundance signature can be preserved: (1) How much does the initial mixing of multiple Pop III SN ejecta dilute this signature? And, (2) how long does it take for Pop II SNe to erase the Pop III chemical signature?

We answer these questions with the following framework. Consider two types of SNe, a normal type n and a special type s . Let p_s be the probability that a given SN is special. Then the yields from SN i are given by:

$$\mathbf{y}_i = \begin{cases} \mathbf{y}_s & \text{probability } p_s \\ \mathbf{y}_n & \text{probability } 1 - p_s, \end{cases} \quad (2)$$

where \mathbf{y}_i is the vector of metal yields for SN i in units of solar masses (*not* the mass fraction). In this paper, \mathbf{y}_n will always denote the metal yields from standard Pop III CCSNe (i.e. the first column of Tables 2 and 3). \mathbf{y}_s will be the metal yields for faint SNe, wind+SNe, or PISNe.

To determine the fraction of stars preserving the special signature during the initial enrichment period, we run these yields through an enrichment model that determines the metallicity of second-generation stars. We consider a mass M_{mix} within which the gas is chemically homogeneous due to turbulent mixing. If the j th second-generation star is enriched by N_j Pop III SNe, then the metallicity \mathbf{Z}_j is given

by

$$\mathbf{Z}_j = \frac{1}{M_{\text{mix}}} \sum_{i=0}^{N_j} q_i \mathbf{y}_i, \quad (3)$$

where $q_i \in [0, 1]$ is the fraction of metals from the i th SN that is mixed into M_{mix} . Depending on the environment, there will be different ways to determine M_{mix} , N_j , and q_i . We describe simple models for these quantities for second-generation star formation in minihaloes (Section 3.1) and atomic cooling haloes (Section 3.2).

To examine question (1), we simplify the problem as follows. For a given metallicity \mathbf{Z}_j , we classify the star as special or normal depending on its metal ratios. When investigating the CEMP signature, we consider the star to be special if $[C/Fe] > 0.7$. When investigating the PISN signature, we consider the star to be special if $[Co/Ni] < -0.5$. For each value of p_s , we employ a Monte Carlo procedure to run our enrichment model N_{total} times to produce $\{\mathbf{Z}_j\}_{j=1}^{N_{\text{total}}}$. Each of these Monte Carlo realizations represents a chemically homogeneous star cluster, of which N_s star clusters are classified as special. Then we define the preservation fraction f_s to be the fraction of these star clusters that retain the special signature:

$$f_s(p_s) = \frac{N_s}{N_{\text{total}}}, \quad (4)$$

where we have made explicit the dependence of f_s on the input probability for special yields, p_s . The function $f_s(p_s)$ in different environments thus describes how well a special signature is preserved, depending on the likelihood for special SNe to occur. In this paper we use $N_{\text{total}} = 10^5$ throughout.

To answer question (2), in Section 3.3, we describe when the contribution from Pop II SNe is able to erase the unique Pop III signature.

3.1 Second-generation star formation in minihaloes

All Pop III SNe in a minihalo explode near the centre, driving a cumulative blastwave. If fallback occurs and triggers second-generation star formation, some fraction of the metals from each SN will enrich this second generation (Ritter et al. 2012; Jeon et al. 2014). When modeling the chemical abundances of metal poor stars, the most common assumption is that metals from different SNe stay completely unmixed, and abundance ratios reflect yields from a single SN (e.g. Joggerst et al. 2010; Nomoto et al. 2013). This idealized case implies $f_s(p_s) = p_s$. However, as we argued in Section 2, this is likely not the generic case, even in minihaloes. In general, $\sim 1 - 10$ SNe will enrich a minihalo. We select N_j from the distributions in Figure 2.

To mix multiple SNe, the simplest assumption is that all metals from all SNe completely mix into some gas mass (e.g. Tinsley 1980; Cooke & Madau 2014). In the language of Equation 3, this fully-mixed model implies $q_i = 1$ for all SNe.

However, a more interesting and likely case is that not all metals from each SN will fall back. Ritter et al. (2015) investigate the scenario of recollapse in a minihalo after seven SNe have exploded in the centre. About half the SN ejecta escape from the halo, suggesting a similar fraction of the

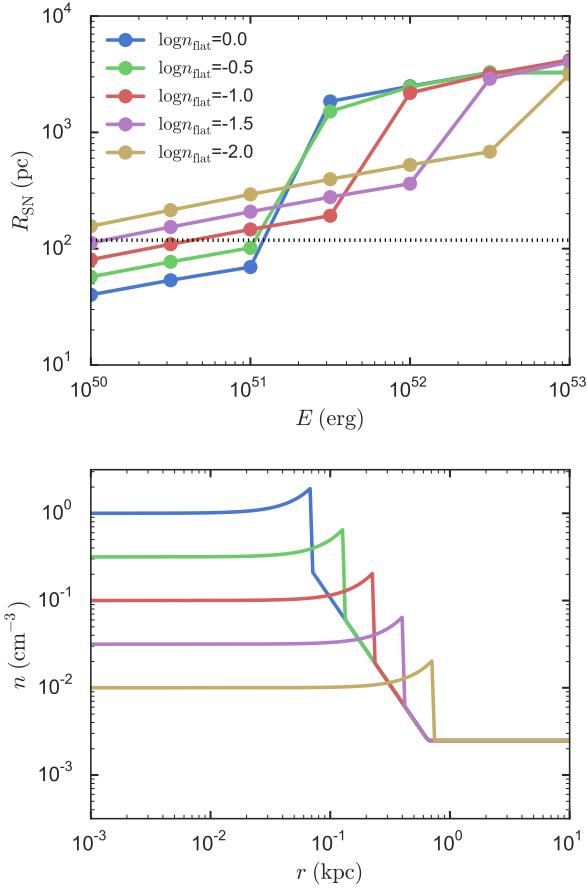


Figure 4. Top: SN bubble final radius expanding out of a minihalo as a function of initial energy deposited and ionizing feedback. The ionizing feedback is parametrized in terms of n_{flat} , which is the flat density in the inner part of the champagne solution. The dotted line indicates the virial radius of the minihalo. Bottom: density profiles for different n_{flat} . The temperature is 10^4 K throughout, which affects the gas pressure.

metal mass escaping. The recollapsing gas in these simulations is biased towards metals from the first SNe to explode in the minihalo, since this ejecta runs into a denser surrounding medium and thus is able to cool faster. The difference in fallback is a factor of 2 – 3 between the first and last star to explode. The amount of metal fallback depends on the details of star formation, stellar feedback, and hydrodynamics in each minihalo. This suggests that a stochastic model is required to describe the amount of fallback. For simplicity, we model q_i in the partial metal fallback case as a random variable uniformly distributed between 0 and 1. To approximate the effect of different SN energies, we also consider a biased case where all the metals from faint SNe are retained in the minihalo ($q_i = 1$ if the i th SN is special), but the normal SNe only retain a uniformly distributed fraction of their metals ($q_i \sim \text{Unif}[0, 1]$ if the i th SN is normal). A suite of more detailed calculations of metal mixing and fallback such as those suggested in Ritter et al. (2015) may find that other fallback distributions are more realistic.

3.2 Second-generation star formation in atomic cooling haloes

Metal enrichment for second-generation star formation in an ACH is a complex process that generally requires a full hydrodynamic simulation (e.g. Greif et al. 2010; Wise et al. 2012; Jeon et al. 2015). However, given the significant parameter uncertainties in Pop III star formation, we here describe a much simpler model that captures the physical nature of this process. The model is illustrated in Figure 3.

Consider an ACH of virial mass $M_{\text{ACH}} \sim 10^8 M_{\odot}$ that virializes at $z_{\text{vir}} = 10$. If we trace all particles within the ACH to higher redshift, there is an associated Lagrangian volume that encompasses all the mass within the ACH at z_{vir} . We call this volume the *ACH Lagrangian Volume*, or ALV for short. This Lagrangian volume is conceptually the same Lagrangian volume that is sampled at high-resolution in a zoom-in simulation (e.g. Safranek-Shrader et al. 2014b). If the Lagrangian volume is spherical, there is some Lagrangian radius $R_{\text{L,ACH}}$ such that

$$R_{\text{L,ACH}} = \left(\frac{3M_{\text{ACH}}}{4\pi\rho_m} \right)^{1/3}, \quad (5)$$

where ρ_m is the total matter density evaluated at some redshift. The physical size of this Lagrangian radius at z_{vir} is found by using $\rho_m(z_{\text{vir}})$, giving $R_{\text{L,ACH}} = 11.4$ kpc.

Now consider the volume \mathcal{V} surrounding and including the ALV. We assume that star-forming minihaloes form uniformly distributed within \mathcal{V} , the SNe in these minihaloes explode independently, and the spherical SN remnant bubbles do not interact with each other hydrodynamically. Given the density of star-forming minihaloes n , the number of minihaloes in the volume \mathcal{V} is given by a Poisson distribution with mean $n\mathcal{V}$. We draw N_j from this Poisson distribution.

Turbulence in the ACH will uniformly mix metals in much of the ACH gas (Greif et al. 2010), but not all the gas within the ACH is well-mixed (i.e. $M_{\text{mix}} \leq f_b M_{\text{ACH}}$). We show in Section 3.2.2 that $M_{\text{mix}} \sim 3 \times 10^6 M_{\odot}$. The Lagrangian volume corresponding to the mixed gas is correspondingly smaller. We call this volume the *Mixed Lagrangian Volume*, or MLV. The radius of the MLV is denoted R_L , a smaller radius than $R_{\text{L,ACH}}$.

For a single minihalo, the fraction of its metal content that is mixed into the MLV can be estimated by calculating the volume overlap between its SN bubble and the Lagrangian volume of the MLV. In other words, if the i th SN bubble has radius R_i , the MLV has radius R_L , and the centre of the minihalo is located at a distance d_i from the centre of the MLV, then

$$q_i = \frac{V_o}{4\pi/3 R_i^3} \quad (6)$$

where the overlap volume V_o can be found by simple geometry and is given by

$$V_o = \begin{cases} 0 & d_i > R_{\text{sum}} \\ \frac{\pi(R_{\text{sum}} - d_i)^2(d_i^2 + 2d_i R_{\text{sum}} - 3R_{\text{diff}}^2)}{12d_i} & R_{\text{diff}} < d_i < R_{\text{sum}} \\ \frac{4\pi}{3} R_i^3 & d_i < R_{\text{diff}} \end{cases}, \quad (7)$$

where $R_{\text{sum}} = R_L + R_i$ and $R_{\text{diff}} = |R_L - R_i|$. For each minihalo, we draw d_i from a uniform 3D spatial distribution, where the maximum distance is given by taking \mathcal{V} as a

sphere. A uniform distribution is appropriate as the distance is considered prior to the collapse of the ACH (see Figure 3). Although the SN bubble radius expands with time, we do not consider the time dependence and instead let the radius instantaneously expand to its final (fixed) radius, only depending on the SN explosion energy. This is further explained in Section 3.2.1.

Other than p_s , the only parameters needed are n and \mathcal{V} . We choose n so that \bar{N}_{MH} , the mean number of minihaloes whose centre is in the ALV, is 10, 30, and 100. This corresponds to $n \approx 0.0016, 0.0048,$ and 0.016 minihaloes per kpc^3 at $z = 10$. We choose \mathcal{V} to be a sphere around the MLV whose radius is 3.5 kpc larger than the MLV (8 kpc when we increase the SN bubble radius beyond that). Since the number of SNe is Poisson, the exact choice of \mathcal{V} does not matter as long as it is large enough to enclose $R_L + R_i$.

In practice, the mass of the SN bubble is likely concentrated in a thin shell, and mixing into the spherical volume depends on the development of Rayleigh–Taylor instabilities (Madau et al. 2001). If no such instabilities develop and all the metals are concentrated in the shell, the overlap fraction is instead determined by the overlapping solid angle, given by:

$$q_i = \begin{cases} 0 & d_i > R_{\text{sum}} \\ \frac{2R_i d_i - d_i^2 - R_i^2 + R_L^2}{4R_i d_i} & R_{\text{diff}} < d_i < R_{\text{sum}} \\ 1 & d_i < R_{\text{diff}} \end{cases} \quad (8)$$

We have checked that using the thin-shell formula does not make a significant difference in our results.

Since multiple SNe explode in each minihalo, for each SN bubble we combine the yields from $\sim 1 - 10$ SNe with the $M_* = 100M_\odot$ number distribution in Figure 2.

3.2.1 Supernova bubble radius

To calculate the size evolution of a Pop III SN bubble, we use the thin-shell approximation in an NFW halo (Madau et al. 2001). We consider haloes of mass $10^6 M_\odot$ virializing at $z = 25$. The NFW concentration parameter is determined using the model from Correa et al. (2015) to be 2.6, although note that minihaloes are strongly triaxial and a spherical NFW density may not properly characterize the gravitational potential (Sasaki et al. 2014). Different concentrations do not greatly affect the bubble radii.

To properly model the gas density profile, we must account for ionizing radiation from the Pop III progenitor stars (Bromm et al. 2003). To approximate the typical gas density profile resulting from ionizing radiation, we use the self-similar champagne flow solution of Shu et al. (2002) as implemented by Wang et al. (2012). We parametrize the self-similar scale using n_{flat} , the density in the inner region. A larger n_{flat} corresponds to a smaller stellar lifetime (Alvarez et al. 2006). Outside of the shock, we use an isothermal profile ($\rho \propto r^{-2}$), evaluated at the halo virial temperature. When the isothermal halo density reaches the ambient IGM value, we prevent it from decreasing further. We use a gas temperature of 10^4 K throughout, corresponding to ionized gas since the HII region outpaces the SN blast wave. We use the cooling function of Sutherland & Dopita (1993) for collisional ionisation equilibrium with $[\text{Fe}/\text{H}] = -3.0$. The bubble is initialized with a Sedov–Taylor solution at 10^4 yr.

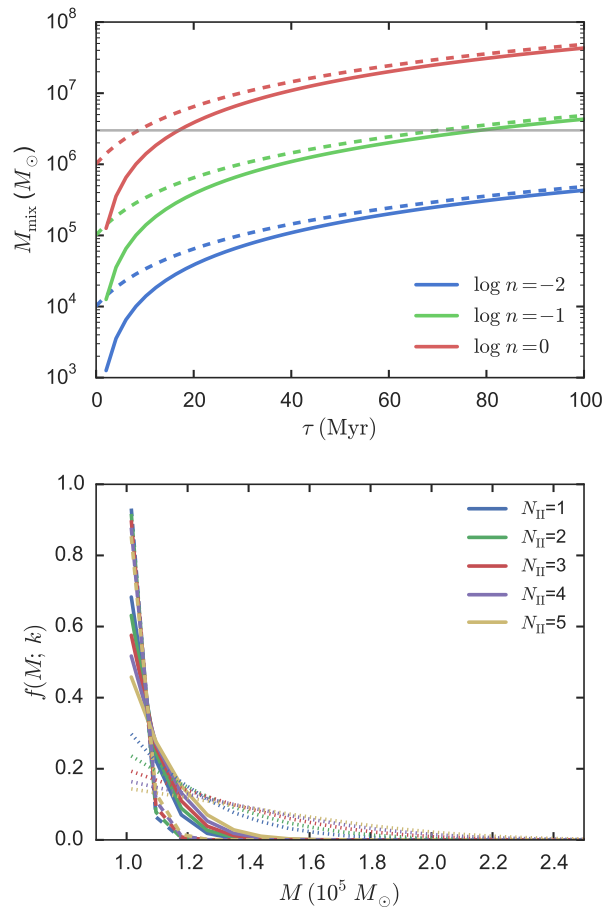


Figure 5. Top: mixing mass within an atomic cooling halo. Solid lines indicate the mixing due to turbulent diffusion, which we use to determine the MLV. Light gray line indicates our choice for the MLV of $3 \times 10^6 M_\odot$. Dashed lines indicate how the mixing mass changes if including a SN bubble of 200 pc, which is relevant for calculating the Karlsson (2005) model. Bottom: mixing mass distributions for the three Pop II star formation rates in the bottom panel of Figure 2. Solid, dashed, and dotted lines correspond to models A, B, and C respectively. k is the number of Pop II SNe enriching a given low mass star. All distributions are roughly between $1 - 2 \times 10^5 M_\odot$.

Unlike the original Madau et al. (2001) model, we include only one SN burst, so we do not include the time-dependent mechanical luminosity term. Instead, SNe contribute their energy to the initial energy of the SN bubble. We take the stopping radius to be the point where the shock velocity is equal to the sound speed in the photoionized medium ($T = 10^4$ K). Although this model is simple, it reproduces the more detailed calculations of Greif et al. (2007), where the SN bubble stalls at 2.5 kpc for a 10^{52} erg explosion in a $5 \times 10^5 M_\odot$ minihalo.

The results are shown in Figure 4. The top panel shows the SN bubble radius as a function of total energy in the bubble, while the bottom panel shows the gas density profiles that the bubble pushes against. Not shown is the underlying NFW profile, which slows the bubble gravitationally. If a bubble is energetic enough to break past the champagne flow shock, it is able to travel much further into the IGM before stopping. In all cases with $E \leq 10^{52.5}$ erg, the bubbles

reach their maximum radius in less than 100 Myr. Since the time delay between Pop III star formation and virialization of the ACH is ~ 100 Myr (see Figure 1), this justifies using an instantaneous bubble size in our ACH enrichment model. Based on Figure 4, a good fiducial radius for a 10^{51} erg CCSN explosion is $\sim 0.2 - 0.4$ kpc, while a 10^{52} erg PISN explosion reaches ~ 3 kpc. We use 0.2 kpc and 3 kpc as the initial radius for CCSNe and PISNe, respectively. However, if the SN bubble expands far enough from the minihalo to be swept up by the ambient Hubble expansion, the radius can grow by a factor of up to 2.5. The maximum extent of the SN bubbles will then be 1 kpc and 7.5 kpc for CCSNe and PISNe, respectively. We show models using these larger radii as well.

3.2.2 Mixing mass

The size of the Mixed Lagrangian Volume in an atomic cooling halo is primarily determined by the extent of turbulent diffusion (Greif et al. 2010). To model this, we use the mixing volume formula from Karlsson et al. (2008)

$$V_{\text{mix}}(\tau) = \frac{4\pi}{3} (6D_t\tau)^{3/2} \quad (9)$$

where τ is the time over which turbulent diffusion occurs, and D_t is the turbulent diffusion coefficient. The factor of 6 is a combination of a factor of 2 from the 1D solution to the diffusion equation and a factor of 3 from three spatial dimensions (Karlsson et al. 2013). The turbulent diffusion coefficient is given as

$$D_t \sim \langle v_{\text{turb}} \rangle \ell_{\text{turb}} / 3 \quad (10)$$

where v_{turb} is a typical turbulent driving velocity, and ℓ_{turb} is a typical turbulent driving scale. This is an order-of-magnitude estimate based on dimensional grounds, similar in nature to that used by mixing length theory to describe convective transport in stars where the mixing length is parametrized in terms of a characteristic scale height (e.g. Kippenhahn et al. 2012). Since turbulence is driven by gravity in our haloes (Wise & Abel 2007; Greif et al. 2008; Safranek-Shrader et al. 2012; Ritter et al. 2015), we estimate that the characteristic v_{turb} is given by the halo virial velocity, and the characteristic ℓ_{turb} is given by a fraction of the virial radius $\sim R_{\text{vir}}/10$. Values for the diffusion coefficient are given in Table 1. The mixing mass as a function of τ and the ambient gas density are shown in Figure 5.

A typical gas density in an atomic cooling halo is $n \sim 10^{-1} \text{ cm}^{-3}$, and a typical amount of time for the gas to be turbulently mixed is the halo free fall time, $t_{\text{ff}} \approx 0.1/H(z) \approx 70 \text{ Myr}$ for $z = 10$. This results in a typical mixing mass of $M_{\text{mix}} = 3 \times 10^6 M_{\odot}$ of gas, or $R_L = 6.4 \text{ kpc}$.

Note that there is in principle a lower bound to the size of the MLV, since a single star cluster is chemically homogeneous (e.g. Bland-Hawthorn et al. 2010; Feng & Krumholz 2014). In the Milky Way this is empirically found to be $\sim 10^5 M_{\odot}$, but it could be lower in the earliest galaxies (Safranek-Shrader et al. 2014b).

3.3 Contamination by Pop II supernovae

Since Pop II CCSNe and standard Pop III CCSNe produce similar metal yields, it may be difficult to distinguish true

second generation stars from low mass stars that have been contaminated by Pop II SNe. This can happen in massive minihaloes as well as in atomic cooling haloes, where potential wells are sufficiently deep to retain their gas if SN feedback is not too strong. At this point, the halo is massive enough to constitute a self-enriching system, a characteristic of a first galaxy (Bromm & Yoshida 2011). To answer question (2), how quickly Pop II SN can erase unique Pop III signatures, we add Pop II SNe one at a time until the signature is wiped out. Here, as before, it is important to know how much gas the SN ejecta mixes into.

For a massive minihalo, in our spherically symmetric model a single 10^{51} SN fills the entire virial radius. Thus we can instantly mix the Pop II SNe into the entire minihalo volume. For simplicity, we assume the total gas mass available is the same as in the original minihalo, although in principle gas will be continually accreted.

In an atomic cooling halo, the mixing mass for an individual SN is often assumed to be the maximum radius of a supernova remnant (e.g. Ryan et al. 1996). However, turbulent mixing can expand the mixing mass. To estimate the size of this effect, we use the Karlsson (2005) model to calculate mixing mass distributions using the three Pop II star formation models in Figure 2. We employ the mixing volume formula from Karlsson et al. (2008), which is similar to Equation 9 but now accounts for the initial SN bubble size R_{SN} :

$$V_{\text{mix}}(\tau) = \frac{4\pi}{3} (6D_t\tau + R_{\text{SN}}^2)^{3/2}. \quad (11)$$

We use $R_{\text{SN}} = 200 \text{ pc}$ from Figure 4, and $n = 0.12 \text{ cm}^{-3}$ and $D_t = 7 \times 10^{-4} \text{ kpc}^2 \text{ Myr}^{-1}$ from Karlsson (2005). The results for a small number N_{II} of Pop II SNe are plotted in Figure 5. Increasing N_{II} allows for slightly higher mixing masses, but the typical mixing masses are $1 - 2 \times 10^5 M_{\odot}$, only slightly larger than the mixing mass right after the SN bubble stops expanding. Lowering the star formation rate by a factor of 10 only slightly increases the maximum mixing mass here to $\sim 3 \times 10^5 M_{\odot}$. Thus, it is reasonable to assume that the mixing volume for Pop II SNe is about the mass of its SN remnant, which we take to be $3 \times 10^5 M_{\odot}$ to maximize the dilution. It is only at larger N_{II} that the effect of turbulent mixing will be important.

We can also come to the conclusion that turbulent mixing is relatively unimportant by estimating the time-scale for turbulent mixing to dominate the mixing volume in Equation 11. This is approximately when

$$\tau = \frac{R_{\text{SN}}^2}{6D_t} \approx 27 \text{ Myr} \left(\frac{R_{\text{SN}}}{200 \text{ pc}} \right)^2 \left(\frac{D_t}{10^{-3} \text{ kpc}^2 \text{ Myr}^{-1}} \right)^{-1} \quad (12)$$

This time-scale is longer or comparable to the ~ 10 Myr recovery time in a self-enriching system, so turbulent mixing will not affect the mixing mass by more than a factor of a few.

4 RESULTS

We now present model calculations showing how well the CEMP (Section 4.1) and PISN (Section 4.2) chemical signatures are preserved in gas from which metal-poor stars would form in the early Universe. We inject a natal fraction p_s of

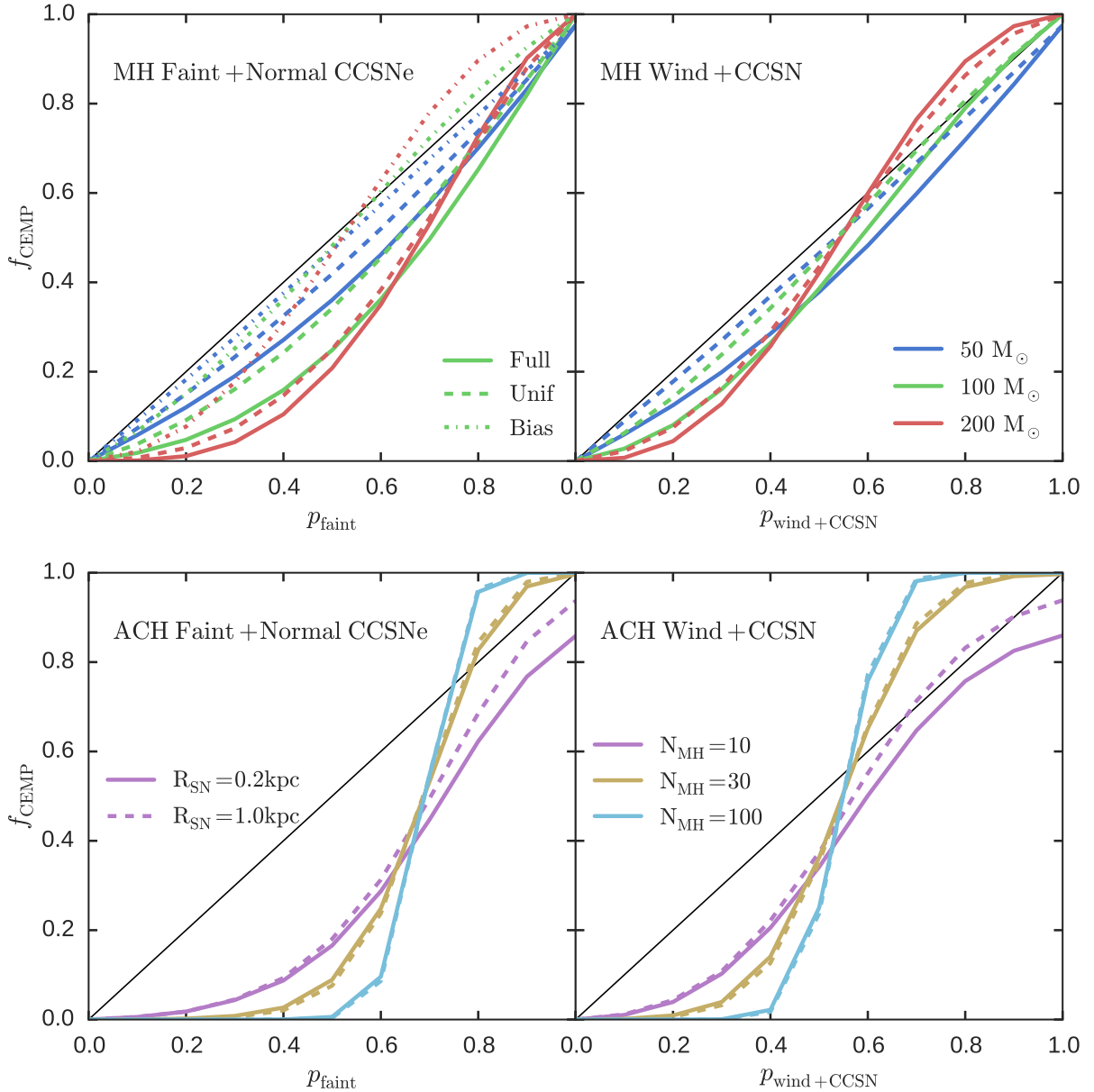


Figure 6. CEMP signature preservation in star-forming haloes after the addition of metals by Pop III SNe. Top row: Minihalo models are shown. The solid, dashed, and dot-dashed lines indicate different amounts of SN ejecta fallback into the; minihalo. Different colours indicate different total mass of Pop III stars formed per minihalo, which translates into the SN number distributions in Figure 2. Overall, the observed f_{CEMP} in second-generation stars reflects the input special fractions p_s . Bottom row: atomic cooling halo models are shown. The solid and dashed lines indicate different SN bubble sizes. Different colors indicate different values for the mean number of minihaloes contributing metals to an ACH. In both cases, f_{CEMP} rapidly changes from 0 to 1 over a narrow range of input p_s . See text for more discussion.

special Pop III yields along with $1 - p_s$ of normal Pop III CCSN. We process this through our mixing models (see Section 3), and calculate the fraction f_s of stars retaining the special Pop III signature. We consider the preservation both during the initial enrichment by combining multiple Pop III SNe, as well as after adding Pop II SNe. In Section 4.3, we compare our models from Section 4.1 to the observed stellar halo CEMP star fraction.

4.1 Preserving a CEMP signature

As a reminder, we say a metal-poor star displays the *CEMP signature* if it has $[\text{C}/\text{Fe}] > 0.7$. The input special fraction p_s will refer to two different models for producing the CEMP signature in Pop III stars. If p_s is p_{faint} , then we combine faint and normal CCSNe to produce the CEMP signature. If p_s is $p_{\text{wind+CCSN}}$, then we add a carbon wind to the yields of some of the CCSNe to produce the CEMP signature.

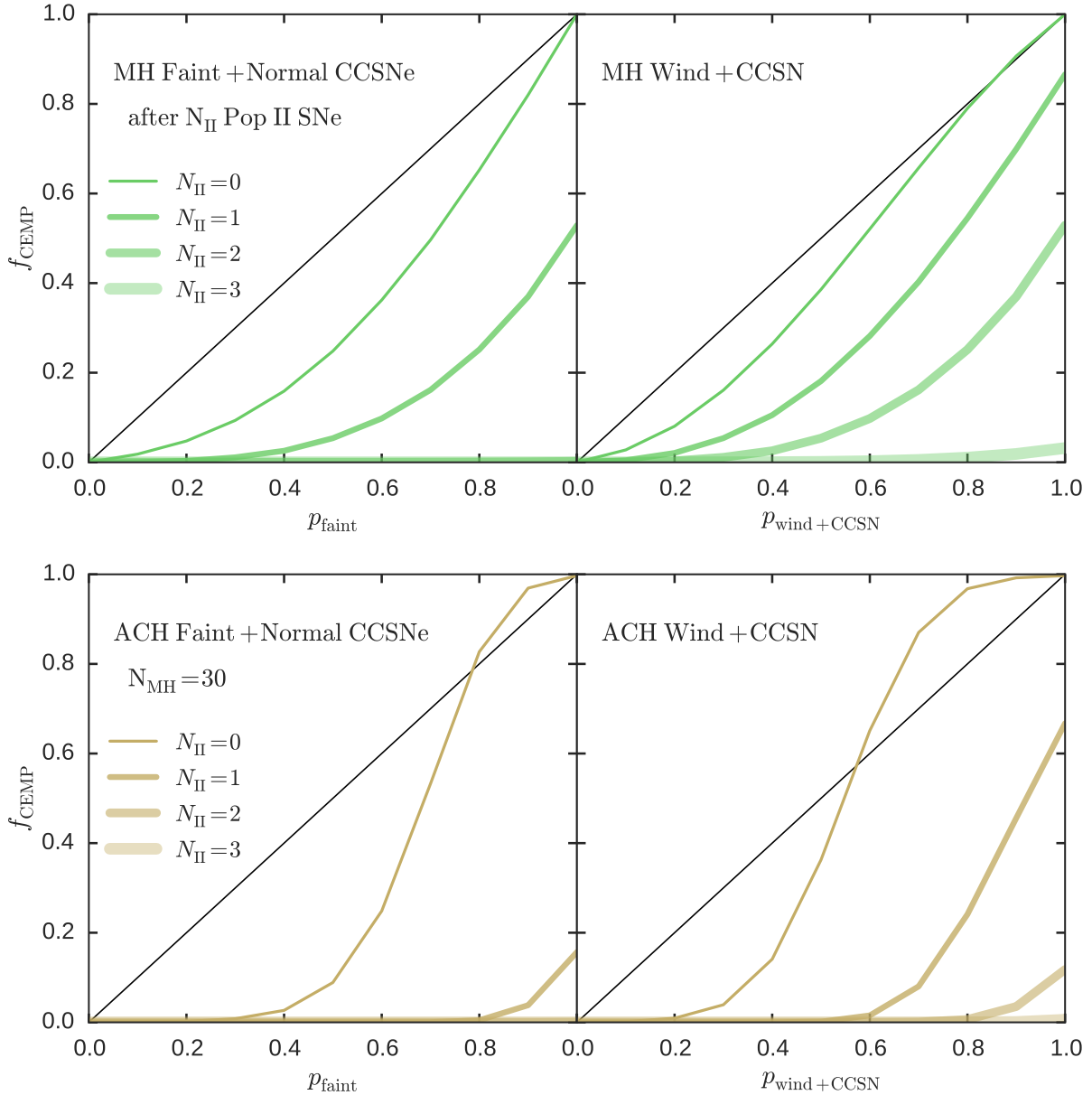


Figure 7. CEMP signature preservation after dilution by N_{II} Pop II SNe. Panels are arranged as in Figure 6. Different line thickness and transparency denote different numbers of Pop II SNe. The MH lines show deviations from the model using $M_* = 100M_{\odot}$ of Pop III stars per minihalo and full metal fallback in the minihalo after adding Pop II SNe. The ACH models show deviations from the model using $R_{\text{SN}} = 200 \text{ pc}$ and $\bar{N}_{\text{MH}} = 30$. In all models, only a few Pop II SNe are required to eliminate the CEMP signature, even if 100 per cent of Pop III stars produce the CEMP signature. Note that in several panels, the larger N_{II} lines are at $f_{\text{CEMP}} \approx 0$ regardless of p_s and thus are barely visible at the bottom of the panels.

4.1.1 Multiple Pop III SNe

In Figure 6, we show the preservation fraction for the CEMP signature in the MH and ACH environments (top and bottom rows, respectively) assuming the signature is generated through either the faint+normal CCSNe or the wind+CCSN mechanisms (left and right columns, respectively). As an example of interpreting the figure, consider the model of faint+normal CCSNe in a MH (top-left corner). Suppose $p_{\text{faint}} = 0.6$, i.e. 60 per cent of *all* Pop III SNe are faint CCSNe and 40 per cent are normal CCSNe. Then the solid green line shows that if minihaloes form a combined $100M_{\odot}$

of Pop III stars and all the metals fully mix ($q_i = 1$), then ~ 35 per cent of metal-poor stars forming in minihaloes will retain the CEMP signature. For reference, the thin black line in the plots indicates where $f_{\text{CEMP}} = p_s$, or where the CEMP signature has been perfectly preserved. We stress that all the second-generation stars in any given minihalo will have the same signature, since they form from a chemically homogeneous star cluster (Ritter et al. 2015; Safranek-Shrader et al. 2015).

In the top row of Figure 6 we show the CEMP signature preservation fraction for the minihalo models. In general, the MH Wind+CCSN models are within ~ 10 per cent

of perfect preservation. However, the faint+normal CCSNe models can deviate strongly from perfect preservation. In particular, at low p_{faint} and larger numbers of Pop III SNe, the CEMP signature is strongly suppressed. This is simply because it is easier to reduce the $[\text{C}/\text{Fe}]$ ratio by adding iron from the normal CCSNe to the iron-poor faint CCSNe. As expected, having biased fallback for faint SNe (dot-dashed lines) results in much better signature preservation.

In the bottom row, we show the CEMP signature preservation fraction for the atomic cooling halo models. The solid and dashed lines show SN expansion radii of 200 pc and 1 kpc, showing the range of preservation fractions based on whether the Hubble flow expands the SN bubbles. The colors indicate different numbers of minihaloes that contributed metals to the ACH. Recall that each minihalo in these models can produce multiple CCSNe, where the number is drawn from the green $100M_{\odot}$ distribution in the top panel of Figure 2. While the MH models reasonably preserve the Pop III signature regardless of p_s , the ACH models show a sharp transition from poorly preserved to over-preserved. This is due to the average $[\text{C}/\text{Fe}]$ ratio in all haloes being determined by p_{faint} . As we increase the number of SNe contributing metals to a gas reservoir (MH or ACH), the abundance scatter between different gas reservoirs decreases, resulting in a larger fraction of the gas reservoirs being close to the average value. Note that in the $\bar{N}_{\text{MH}} = 10$ case, when p_{faint} and $p_{\text{wind+CCSN}} = 1$ there is still not perfect preservation. This occurs because of cases where all minihaloes are within the ALV but do not intersect the MLV.

Overall, it is generally the case that the CEMP signature can be preserved in the gas after combining yields from multiple Pop III SNe in MHs. It is difficult but not impossible to preserve the signature in ACHs. However, even if second-generation low-mass stars can be identified from observations of metal-poor stars, our models show that the observed CEMP star fraction will generally be slightly lower than the actual fraction of Pop III SNe producing the CEMP signature. A metal enrichment model (such as the one used to calculate Figure 6) is required to convert observed CEMP star fractions into the actual fraction of Pop III SNe producing the CEMP signature.

4.1.2 Adding Pop II SNe

In Figure 7, we show how the preservation signature is kept after adding Pop II SNe yields to the metal distributions from Figure 6. Each Pop II SN yield is diluted into $3 \times 10^5 M_{\odot}$, which we have conservatively chosen to be on the high end of possible dilution masses. Interestingly, in all four cases, adding 1–3 Pop II SNe is enough to erase the CEMP signature in the gas as imprinted by Pop III SNe. In the MH case, this is because the signature is already close to being erased by a few normal Pop III CCSNe. In the ACH case, it is a result of the ~ 10 times discrepancy in the mixing mass between Pop III and Pop II SNe.

A typical Pop II burst in these environments produces $\sim 1000M_{\odot}$ of stars. For a Salpeter IMF, there are ~ 5 massive stars that explode as SNe in the first Pop II star formation burst. As a consequence, this strongly suggests that if CEMP stars trace Pop III nucleosynthesis, they are truly second-generation stars that form out of only Pop III metals (although multiple Pop III stars will contribute metals).

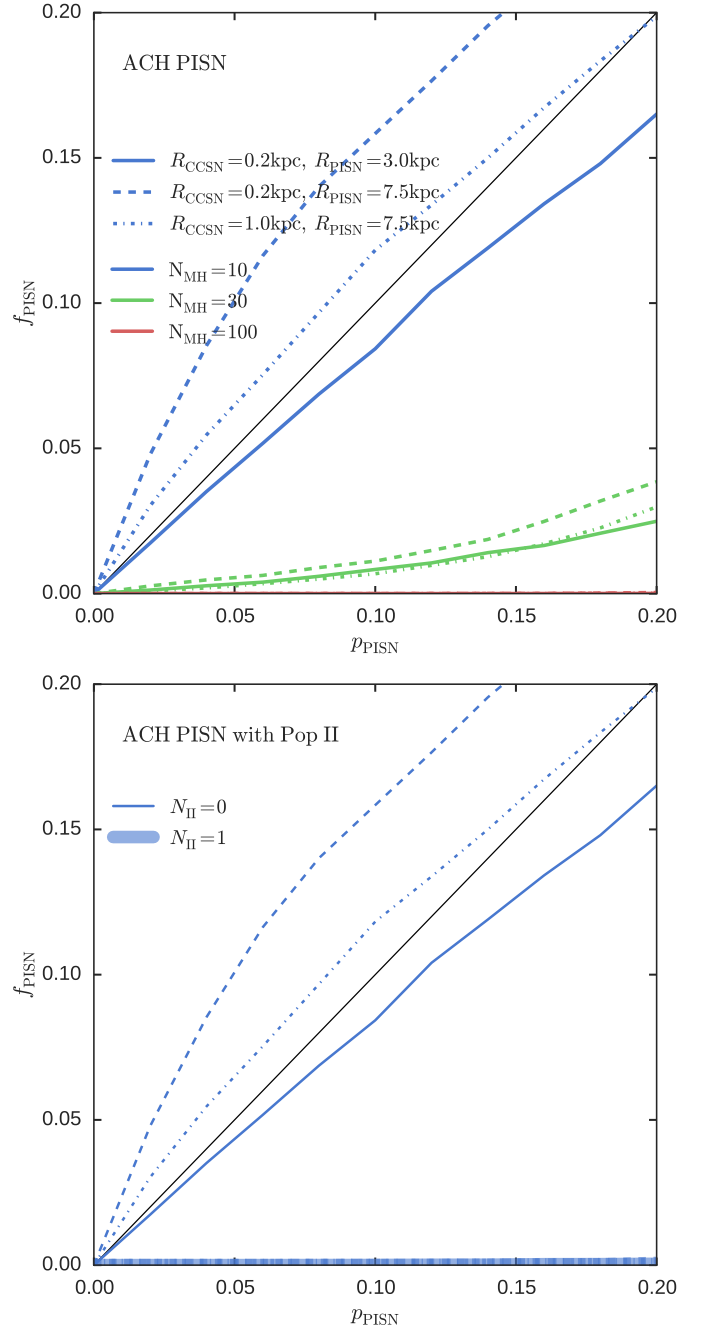


Figure 8. PISN signature preservation in the ACH model. Top: Pop III only. The line colors indicate different values for the mean number of minihaloes. Solid, dashed, and dot-dashed lines indicate different SN bubble radii. The thin black line denotes perfect preservation. If a minihalo experiences a PISN, that is the only SN in the minihalo. If it has CCSNe, then the number of CCSNe is drawn from the $100M_{\odot}$ distribution of Figure 2. Note that p_{PISN} only extends from 0.0–0.2, as we do not expect most minihaloes to host PISNe. Bottom: after adding a single Pop II SN, the PISN signature is erased. The $N_{\text{II}} = 1$ line has $f_{\text{PISN}} \approx 0$ for all shown p_{PISN} and is thus barely visible at the bottom of the plot.

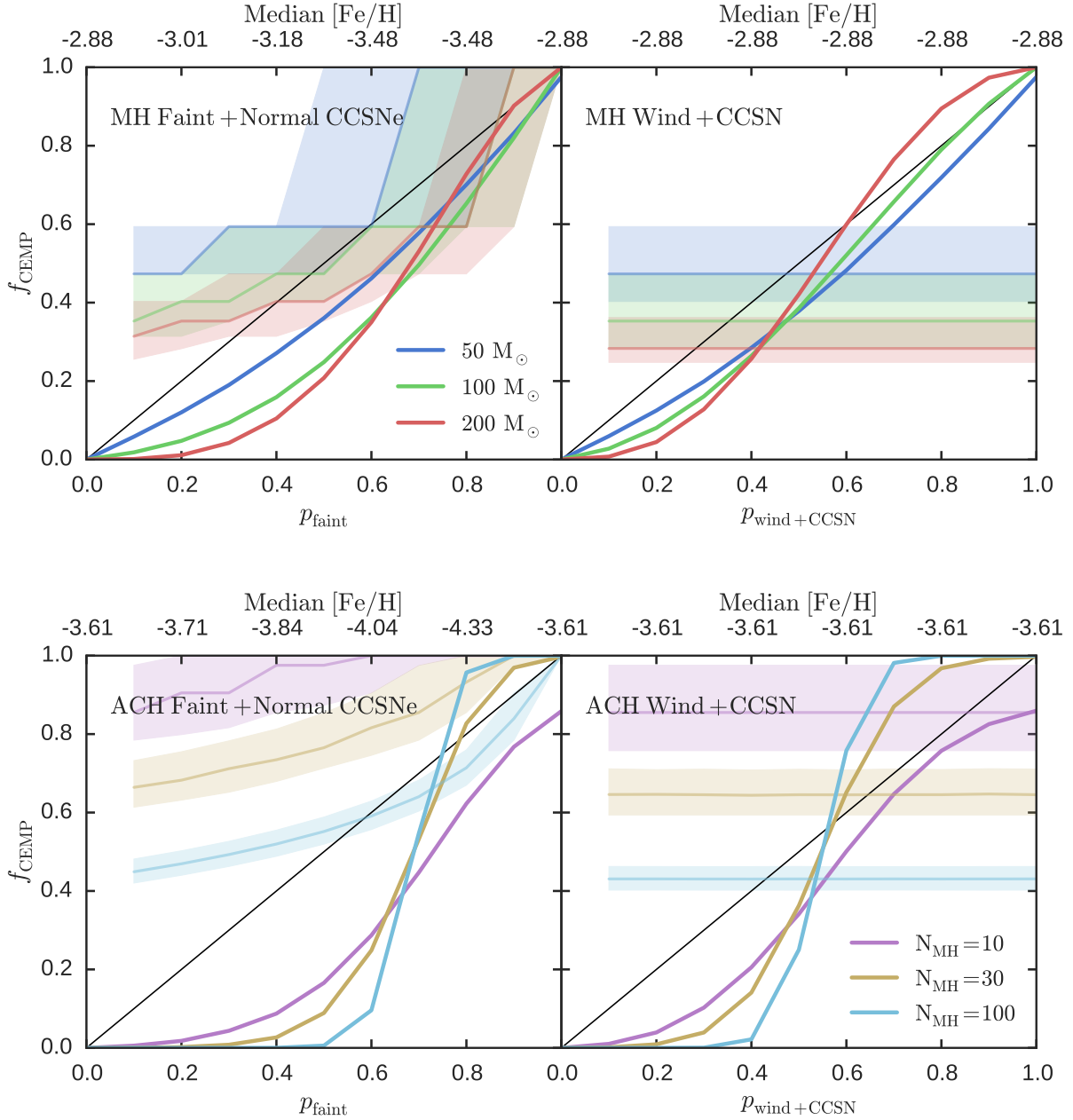


Figure 9. CEMP signature preservation compared to expected CEMP star fractions based on model $[\text{Fe}/\text{H}]$ and observed CEMP star fractions (Equation 13). Shaded regions show the 25 and 75 percentile of the model $[\text{Fe}/\text{H}]$ distributions translated into observed CEMP star fractions, with light solid line showing the median value. The median $[\text{Fe}/\text{H}]$ for the $100M_{\odot}$ and $\bar{N}_{\text{MH}} = 30$ models are shown on the top axis of each panel. Panels are arranged as in Figure 6. For the MH panels, we only show the full fallback case. For the ACH panels, we only show $R_{\text{SN}} = 0.2 \text{ kpc}$. The values of p_{faint} and $p_{\text{wind+CCSN}}$ where the model lines intersect the shaded bars are consistent with the observed CEMP fraction.

4.2 Preserving a PISN signature

We define a metal-poor star as retaining the PISN signature if it forms from gas with $[\text{Co}/\text{Ni}] < -0.5$. As previously discussed, this is a representative odd-even element abundance ratio. In the top panel of Figure 8, we show the preservation fraction for the PISN signature (f_{PISN}) depending on the fraction of minihaloes hosting PISNe (p_{PISN}). If a minihalo does not host a PISN, it then has a random number of CCSNe drawn from the $100M_{\odot}$ distribution of Figure 2. Models are shown for different SN bubble radii and different

numbers of minihaloes. We only use the ACH model and not the MH model, since the strong PISN explosion evacuates its minihalo of gas (Whalen et al. 2008).

In general, the PISN signature is well preserved for the expected number of 10 minihaloes contributing to the ACH. As more minihaloes are added, the number of normal Pop III CCSNe increases and is able to overwhelm the PISN signature at these low p_{PISN} fractions. Note that when the size of the PISN bubbles is increased, the PISN signature is actually stronger than perfect preservation. This is because

for the same number density of minihaloes (as parametrized by \bar{N}_{MH}), increasing the SN bubble radius allows more such bubbles to overlap with the MLV. The MLV is then able to sample more PISN bubbles than CCSN bubbles. Increasing the size of the CCSN bubbles somewhat counteracts the PISN signature for the same reasons.

The PISN signature is very fragile. The bottom panel of Figure 8 shows that a single Pop II SN is able to wipe out the PISN signature. Again, this is due to the vastly different dilution factors between the Pop III and Pop II SNe.

It is interesting to compare the results of this model to cosmological simulations, such as the one by Jeon et al. (2015). In contrast with many previous simulations, this simulation allows for both PISNe and CCSNe to occur in the minihaloes. By $z \approx 10.5$, 2 PISNe have formed out of a total of ~ 200 Pop III stars, corresponding to $p_{\text{PISN}} \approx 0.01$. These two PISNe contribute the majority of metals in the simulation, but nearly all of these metals are ejected into the IGM rather than found in virialized haloes. Their most massive galaxy is thus predominantly enriched by CCSNe. We also find that the $\bar{N}_{\text{MH}} = 30$ case (similar to their number of minihaloes) has CCSNe dominating the metal enrichment in a typical ACH when $p_{\text{PISN}} = 0.01$.

4.3 Interpreting observations of metal-poor stars

Ultimately, the goal of stellar archaeology is to interpret abundances of metal-poor stars to learn about properties of Pop III stars. We now present an example of how our results in Section 4.1 can be used to interpret observed CEMP star fractions in the Milky Way halo as constraints on Pop III properties.

Let us suppose that the CEMP star fraction in the stellar halo is representative of second-generation stars. In practice, the halo is an amalgam of stars from many sources, and even at fairly low metallicities some halo stars may form after the first few generations. Regardless, with this assumption, we can compare the observed CEMP star fraction to that obtained by our metal enrichment models. Our models give estimates of the $[\text{Fe}/\text{H}]$ distributions of Pop II stars. We take these $[\text{Fe}/\text{H}]$ distributions and find the 25th and 75th percentile values to define a range of f_{CEMP} . We consider models to be allowed if their predicted f_{CEMP} is consistent with the f_{CEMP} computed from the model $[\text{Fe}/\text{H}]$ distributions. For the observed CEMP star fraction, we take an approximate fit to the CEMP fraction from figure 16 of Placco et al. (2014) for $[\text{C}/\text{Fe}] > 0.7$.

$$f_{\text{CEMP}} = \begin{cases} 0.2 & [\text{Fe}/\text{H}] > -2.5 \\ -0.8 - 0.4 \times [\text{Fe}/\text{H}] & -4.5 < [\text{Fe}/\text{H}] < -2.5 \\ 1.0 & [\text{Fe}/\text{H}] < -4.5 \end{cases} \quad (13)$$

In Figure 9 we show the preservation fraction for some of the models in Figure 6. The shaded bars in the background indicate the observed CEMP star fraction evaluated at the modelled $[\text{Fe}/\text{H}]$ distributions. Note that the shaded bars for the wind+CCSN models are flat, since every SN has the same iron yield.

When the model lines overlap the shaded bars, the corresponding p_{faint} or $p_{\text{wind+CCSN}}$ are consistent with the observations. Taking the figure at face value, we see that the MH models produce the expected carbon fractions, although

it generally requires a fairly high p_s . The faint+normal CC-SNe models require $p_{\text{faint}} \gtrsim 0.6$. If this picture is correct, then our results imply that $\gtrsim 60$ per cent of Pop III stars exploded as a faint SN. The high fraction of faint SNe can be interpreted as an indirect tracer of the IMF (e.g. Heger & Woosley 2002). A similar calculation for the biased fallback model suggests that $p_{\text{faint}} \gtrsim 0.5$. If instead the CEMP signature is produced in MHs by carbon winds, the wind+CCSN models require $0.7 \gtrsim p_{\text{wind+CCSN}} \gtrsim 0.4$. This could be interpreted as the fraction of Pop III stars that are rotating rapidly enough to have significant winds.

In contrast, the ACH models seem to be unable to produce consistent CEMP star fractions without a huge number of minihaloes contributing to the ACH. Recall that each minihalo here can produce multiple Pop III SNe, and $\bar{N}_{\text{MH}} = 100$ is a strong upper limit assuming there has been no smooth mass accretion. Thus, if the CEMP signature is created solely by Pop III stars, a large fraction of Pop III stars must produce the high $[\text{C}/\text{Fe}]$ abundances, and most of these stars form in minihaloes.

Given the simplicity of our enrichment models, we caution that more sophisticated models could somewhat affect the exact numbers. In particular, while the overall metallicity in our models is likely correct to within an order of magnitude, the actual value can be shifted by changing the dilution mass within some reasonable range. From Equation 13, a 0.2 dex change in the model $[\text{Fe}/\text{H}]$ results in a 0.08 change in the observed f_{CEMP} . It is also a fairly strong assumption that the observed CEMP stars represent only second-generation stars, although at $[\text{Fe}/\text{H}] \lesssim -3$ it is probably reasonably accurate. However, we can qualitatively see the effect of including subsequent generations of stars. Since the CEMP signature is rapidly erased by Pop II SNe, any contaminating stars will reduce the observed CEMP star fraction. Thus a true second-generation CEMP star fraction will be higher than the shaded bars plotted in Figure 9. This further increases the p_s required to be consistent with the MH models, as well as exacerbating the inability of the ACH models to produce the observed CEMP star fractions. Regardless, this approach of comparing observed special fractions f_s to those found from models is an emerging framework to test where our understanding needs to most improve to constrain properties of Pop III stars.

5 SUMMARY AND CONCLUSIONS

In this study we focused on whether unique Pop III chemical signatures can be preserved in the gas from which the first low mass stars form. Using simple models that capture the essence of initial Pop III chemical enrichment, we calculate the fraction of second-generation stars preserving unique Pop III chemical signatures depending on the input fraction of Pop III stars that produce said signature. We now summarize our main findings and conclusions.

The chemical signature of Pop III can be preserved in gas from which the first low-mass stars formed. Metal-poor stars are believed to trace the nucleosynthetic yields of their progenitor stars which in the case of the most metal-poor ones are individual Pop III SNe events. While this is the fundamental assumption that stellar archaeology rests on, detailed investigations to what extent

SN yield signatures remain intact in the gas after the explosion and factoring in various environmental aspects such as mixing and the presence of multiple SNe are still lacking

Even the very first enrichment step has irreducible complexity, with at least a handful of Pop III SNe contributing metals to most second-generation star forming environments. We find that the mixing and re-accretion of gas onto the halo following these SNe does not always wipe out the original nucleosynthetic signatures, and thus that it is possible for second-generation stars to trace Pop III properties. This validates the endeavor of stellar archaeology. Nevertheless, it becomes increasingly clear that interpreting observed abundance signatures in the most metal-poor stars requires using chemical enrichment models to factor in effects such as metal mixing and turbulence (see also Ritter et al. 2015). Otherwise the properties of Pop III stars may not be correctly recovered.

The frequency of metal-poor stars with a special abundance signature (e.g. high [C/Fe]) cannot be directly interpreted as the fraction of Pop III stars producing that signature. By comparing the results of our MH and ACH models to the observed fraction of CEMP stars in the Galactic stellar halo, we find that CEMP stars likely formed from gas in a minihalo enriched by a SN that underwent metal fallback. The observed high CEMP star fraction is not necessarily produced by faint SNe alone, but if so then the fraction of Pop III stars producing the CEMP signature must be rather high, at least $\sim 40 - 60$ per cent even though the observed CEMP star fractions are lower. This high fraction could be an indication of a biased scenario, such as preferential second-generation star formation in minihaloes that experience low energy SNe (Cooke & Madau 2014). However, a better understanding of the CCSN explosion mechanism is likely necessary to confirm this, as even quite energetic SNe can produce a similar abundance pattern (Tominaga et al. 2007). Either way, it is nearly impossible to reproduce the observed CEMP star fraction in atomic cooling haloes.

Any Pop III chemical signatures are quickly erased after the emergence of Pop II SNe. This fundamental result suggests that stars with unique and unusual chemical abundance signatures are clean probes of Pop III SN yields. This effect has been understood before in the general context of chemical evolution (e.g. Audouze & Silk 1995), but the sheer rapidity with which unique abundance signatures are erased has not been appreciated. Future abundance studies based on high-resolution spectroscopy should focus on any unusual halo stars as they will likely reflect Pop III nucleosynthesis yields. Moreover, stars with $[\text{Fe}/\text{H}] \lesssim -4.0$ of which many show unique abundances can all be regarded second-generation stars. This is in line with other suggestions from SN yield fitting of observed abundance signatures in the most metal-poor stars (Tominaga et al. 2014; Keller et al. 2014; Placco et al. 2015), although these authors also considered stars with halo-like abundances and not just unusual signatures.

A PISN signature is quickly wiped out by the emergence of Pop II SNe. A strong odd-even effect is believed to be a tell-tale sign of a PISN signature. So far, only one star has been identified that displays some degree of an odd-even effect (Aoki et al. 2014). This may suggest that PISNe are exceedingly rare. However, this does not neces-

sarily imply that Pop III *PISN explosions* were equally rare, or even absent. Our results instead suggest that any PISN enrichment pattern would rapidly be hidden under subsequent layers of Pop II core-collapse enrichment. In addition, a PISN signature might only occur in stars with high metallicity since the Ca yield of a PISN is rather large (Karlsson et al. 2008). Current selection biases on the basis of a weak Ca II K line would thus preclude finding these stars. Interestingly, even though PISNe produce large amounts of metals, it appears to be very difficult for most of the PISN metals to be retained in a first galaxy environment that would then lead to the formation of metal-poor stars. This is due to metals being dispersed over a much larger volume compared to those from CCSNe. As previously suggested, the best place to search for the PISN signature may be in IGM gas at high redshifts with absorption spectroscopy (Jeon et al. 2015).

Despite the fact that our enrichment models are idealized and only capture the essence of the problem, our results are encouraging and highly relevant to the interpretation of the abundance signatures of metal-poor stars and thus to the field of stellar archaeology. Hydrodynamic simulations that elucidate the nature of metal mixing and enrichment in the early universe are particularly important. The results from these simulations will allow for more quantitative investigations since our simple models have already demonstrated that one can recover valuable information about Pop III stars from stellar archaeology.

We have shown that it is possible to learn about the nature and properties of Pop III stars by using chemical abundance measurements of metal-poor halo stars, such as in the case of the observed CEMP star fraction. However, the complex formation history of the stellar halo makes it difficult to isolate true second-generation stars. The only way to best choose candidates is to select the lowest metallicity stars, but that may not yield a complete sample since not all second-generation stars may be at the lowest metallicities (see e.g. Frebel & Bromm 2012; Frebel et al. 2014).

A more promising way to find and study second-generation stars may be in dwarf galaxies and to carry out dwarf galaxy archaeology (Frebel & Bromm 2012). As each dwarf galaxy is a single, confined object with one specific history, it will be easier to model the galaxies and to separate second-generation stars from other stars within these galaxies. Of the Milky Way's dwarf galaxies, the ultra-faint dwarfs may be the best places to clearly identify second-generation stars. Their chemical abundances and star formation histories suggest that ultra-faint dwarfs form stars only over a very short period of time (Frebel et al. 2014; Brown et al. 2014), and due to their inefficient star formation, a large fraction of their stars (or even all of them) may be second-generation. If ultra-faint dwarf galaxies were the descendants of a single Pop III star-forming minihalo, each ultra-faint dwarf galaxy would only preserve one single combination of Pop III yields. However, if these galaxies are ACHs that form from a merger of more than one second-generation star forming minihalo, then multiple second-generation gas reservoirs may be represented in the dwarf galaxy.

A disadvantage of using stars in dwarf galaxies to constrain properties of Pop III stars is the relatively small number of stars with available chemical abundance observations. High resolution spectroscopy is the gold standard, but the

faintness of most dwarf galaxy stars may require further development of medium resolution techniques (e.g. Vargas et al. 2013, 2014; Kirby et al. 2015) or await the era of extremely large telescopes.

All but the least-luminous ultra-faint dwarfs have experienced some level of extended star formation (Vargas et al. 2013). Thus, for detailed studies of true Pop III signatures, it will be important to separate bona-fide second-generation stars from subsequent star formation. A promising approach may be to combine different Pop III yields and enrichment models with chemical evolution models that account for hierarchical galaxy formation (e.g. Salvadori et al. 2015). These models will need to account for the effects that recent hydrodynamic simulations have highlighted (Ritter et al. 2015; Sluder et al. 2015; Bland-Hawthorn et al. 2015). With a larger sample of available dwarf galaxy abundances and more sophisticated modeling of the formation of these systems, it may become possible to robustly and comprehensively constrain the properties of Pop III stars with dwarf galaxy archaeology.

ACKNOWLEDGEMENTS

APJ thanks Ralf Klessen and Brendan Griffen for helpful conversations, and the UC HiPACC 2014 Summer School for useful lectures. This work has made extensive use of the python libraries `numpy`, `scipy`, `matplotlib`, and `seaborn`. APJ and AF are supported by NSF grant AST-1255160. AF acknowledges support from the Silverman (1968) Family Career Development Professorship. VB is supported by NSF grant AST-1413501.

REFERENCES

- Abel T., Bryan G. L., Norman M. L., 2002, *Science*, 295, 93
- Alvarez M. A., Bromm V., Shapiro P. R., 2006, *ApJ*, 639, 621
- Aoki W., Beers T. C., Christlieb N., Norris J. E., Ryan S. G., Tsangarides S., 2007, *ApJ*, 655, 492
- Aoki W., Tominaga N., Beers T. C., Honda S., Lee Y. S., 2014, *Science*, 345, 912
- Argast D., Samland M., Thielemann F.-K., Qian Y.-Z., 2004, *A&A*, 416, 997
- Audouze J., Silk J., 1995, *ApJ*, 451, L49
- Beers T. C., Christlieb N., 2005, *ARA&A*, 43, 531
- Bland-Hawthorn J., Karlsson T., Sharma S., Krumholz M., Silk J., 2010, *ApJ*, 721, 582
- Bland-Hawthorn J., Sutherland R., Webster D., 2015, *ApJ*, 807, 154
- Bromm V., 2013, *Reports on Progress in Physics*, 76, 112901
- Bromm V., Loeb A., 2003, *Nature*, 425, 812
- Bromm V., Yoshida N., 2011, *ARA&A*, 49, 373
- Bromm V., Coppi P. S., Larson R. B., 2002, *ApJ*, 564, 23
- Bromm V., Yoshida N., Hernquist L., 2003, *ApJ*, 596, L135
- Bromm V., Yoshida N., Hernquist L., McKee C. F., 2009, *Nature*, 459, 49
- Brown T. M., et al., 2014, *ApJ*, 796, 91
- Cen R., Riquelme M. A., 2008, *ApJ*, 674, 644
- Chen K.-J., Heger A., Woosley S., Almgren A., Whalen D. J., 2014, *ApJ*, 792, 44
- Chiaki G., Yoshida N., Kitayama T., 2013, *ApJ*, 762, 50
- Clark P. C., Glover S. C. O., Klessen R. S., 2008, *ApJ*, 672, 757
- Clark P. C., Glover S. C. O., Smith R. J., Greif T. H., Klessen R. S., Bromm V., 2011, *Science*, 331, 1040
- Cooke R. J., Madau P., 2014, *ApJ*, 791, 116
- Cooke J., et al., 2012, *Nature*, 491, 228
- Correa C. A., Wyithe J. S. B., Schaye J., Duffy A. R., 2015, *MNRAS*, 452, 1217
- Couchman H. M. P., Rees M. J., 1986, *MNRAS*, 221, 53
- Feng Y., Krumholz M. R., 2014, *Nature*, 513, 523
- Frebel A., Bromm V., 2012, *ApJ*, 759, 115
- Frebel A., Norris J. E., 2015, *ARA&A*, 53, 631
- Frebel A., et al., 2005, *Nature*, 434, 871
- Frebel A., Johnson J. L., Bromm V., 2007, *MNRAS*, 380, L40
- Frebel A., Simon J. D., Kirby E. N., 2014, *ApJ*, 786, 74
- Gal-Yam A., et al., 2009, *Nature*, 462, 624
- Glover S., 2013, in Wiklind T., Mobasher B., Bromm V., eds, *Astrophysics and Space Science Library* Vol. 396, *Astrophysics and Space Science Library*. p. 103 ([arXiv:1209.2509](https://arxiv.org/abs/1209.2509)), doi:10.1007/978-3-642-32362-1_3
- Greif T. H., 2015, *Computational Astrophysics and Cosmology*, 2, 3
- Greif T. H., Bromm V., 2006, *MNRAS*, 373, 128
- Greif T. H., Johnson J. L., Bromm V., Klessen R. S., 2007, *ApJ*, 670, 1
- Greif T. H., Johnson J. L., Klessen R. S., Bromm V., 2008, *MNRAS*, 387, 1021
- Greif T. H., Glover S. C. O., Bromm V., Klessen R. S., 2010, *ApJ*, 716, 510
- Greif T. H., Springel V., White S. D. M., Glover S. C. O., Clark P. C., Smith R. J., Klessen R. S., Bromm V., 2011, *ApJ*, 737, 75
- Greif T. H., Bromm V., Clark P. C., Glover S. C. O., Smith R. J., Klessen R. S., Yoshida N., Springel V., 2012, *MNRAS*, 424, 399
- Haiman Z., Thoul A. A., Loeb A., 1996, *ApJ*, 464, 523
- Hanke F., Müller B., Wongwathanarat A., Marek A., Janka H.-T., 2013, *ApJ*, 770, 66
- Hartwig T., Bromm V., Klessen R. S., Glover S. C. O., 2015, *MNRAS*, 447, 3892
- Heger A., Woosley S. E., 2002, *ApJ*, 567, 532
- Heger A., Woosley S. E., 2010, *ApJ*, 724, 341
- Hirano S., Hosokawa T., Yoshida N., Umeda H., Omukai K., Chiaki G., Yorke H. W., 2014, *ApJ*, 781, 60
- Hirschi R., 2007, *A&A*, 461, 571
- Hopkins P. F., 2012, *MNRAS*, 423, 2037
- Hummel J. A., Pawlik A. H., Milosavljević M., Bromm V., 2012, *ApJ*, 755, 72
- Iwamoto N., Umeda H., Tominaga N., Nomoto K., Maeda K., 2005, *Science*, 309, 451
- Janka H.-T., Hanke F., Hüdepohl L., Marek A., Müller B., Obergaullinger M., 2012, *Progress of Theoretical and Experimental Physics*, 2012, 010000
- Jeon M., Pawlik A. H., Bromm V., Milosavljević M., 2014, *MNRAS*, 444, 3288
- Jeon M., Bromm V., Pawlik A. H., Milosavljević M., 2015, *MNRAS*, 452, 1152
- Ji A. P., Frebel A., Bromm V., 2014, *ApJ*, 782, 95
- Jogerst C. C., Almgren A., Bell J., Heger A., Whalen D., Woosley S. E., 2010, *ApJ*, 709, 11
- Johnson J. L., Greif T. H., Bromm V., 2008, *MNRAS*, 388, 26
- Karlsson T., 2005, *A&A*, 439, 93
- Karlsson T., Johnson J. L., Bromm V., 2008, *ApJ*, 679, 6
- Karlsson T., Bromm V., Bland-Hawthorn J., 2013, *Reviews of Modern Physics*, 85, 809
- Keller S. C., et al., 2014, *Nature*, 506, 463
- Kippenhahn R., Weigert A., Weiss A., 2012, *Stellar Structure and Evolution*. Springer-Verlag Berlin Heidelberg, doi:10.1007/978-3-642-30304-3
- Kirby E. N., Cohen J. G., Smith G. H., Majewski S. R., Sohn S. T., Guhathakurta P., 2011, *ApJ*, 727, 79
- Kirby E. N., et al., 2015, *ApJ*, 801, 125

- Kobayashi C., Nakasato N., 2011, *ApJ*, 729, 16
- Kobayashi C., Umeda H., Nomoto K., Tominaga N., Ohkubo T., 2006, *ApJ*, 653, 1145
- Limongi M., Chieffi A., 2012, *ApJS*, 199, 38
- Loeb A., Furlanetto S. R., 2013, *The First Galaxies in the Universe*. Princeton University Press, Princeton, NJ
- Mac Low M.-M., Klessen R. S., 2004, *Reviews of Modern Physics*, 76, 125
- Mackey J., Bromm V., Hernquist L., 2003, *ApJ*, 586, 1
- Madau P., Ferrara A., Rees M. J., 2001, *ApJ*, 555, 92
- Maoz D., Mannucci F., Brandt T. D., 2012, *MNRAS*, 426, 3282
- McKee C. F., Ostriker E. C., 2007, *ARA&A*, 45, 565
- Meynet G., Ekström S., Maeder A., 2006, *A&A*, 447, 623
- Meynet G., Hirschi R., Ekstrom S., Maeder A., Georgy C., Eggenberger P., Chiappini C., 2010, *A&A*, 521, A30
- Mezzacappa A., et al., 2014, in Pogorelov N. V., Audit E., Zank G. P., eds, *Astronomical Society of the Pacific Conference Series Vol. 488, 8th International Conference of Numerical Modeling of Space Plasma Flows (ASTRONUM 2013)*. p. 102 ([arXiv:1405.7075](https://arxiv.org/abs/1405.7075))
- Nomoto K., Tominaga N., Umeda H., Kobayashi C., Maeda K., 2006, *Nuclear Physics A*, 777, 424
- Nomoto K., Kobayashi C., Tominaga N., 2013, *ARA&A*, 51, 457
- Norris J. E., et al., 2013, *ApJ*, 762, 28
- O'Shea B. W., Norman M. L., 2007, *ApJ*, 654, 66
- Oey M. S., 2000, *ApJ*, 542, L25
- Oh S. P., Haiman Z., 2002, *ApJ*, 569, 558
- Pan T., Kasen D., Loeb A., 2012, *MNRAS*, 422, 2701
- Placco V. M., Frebel A., Beers T. C., Stancliffe R. J., 2014, *ApJ*, 797, 21
- Placco V. M., Frebel A., Lee Y. S., Jacobson H. R., Beers T. C., Pena J. M., Chan C., Heger A., 2015, *ApJ*, 809, 136
- Planck Collaboration et al., 2015, submitted to *A&A* ([arXiv:1502.00391](https://arxiv.org/abs/1502.00391)),
- Ritter J. S., Safrank-Shrader C., Gnat O., Milosavljević M., Bromm V., 2012, *ApJ*, 761, 56
- Ritter J. S., Sluder A., Safrank-Shrader C., Milosavljević M., Bromm V., 2015, *MNRAS*, 451, 1190
- Ryan S. G., Norris J. E., Beers T. C., 1996, *ApJ*, 471, 254
- Safrank-Shrader C., Agarwal M., Federrath C., Dubey A., Milosavljević M., Bromm V., 2012, *MNRAS*, 426, 1159
- Safrank-Shrader C., Milosavljević M., Bromm V., 2014a, *MNRAS*, 438, 1669
- Safrank-Shrader C., Milosavljević M., Bromm V., 2014b, *MNRAS*, 440, L76
- Safrank-Shrader C., Montgomery M., Milosavljevic M., Bromm V., 2015, submitted to *MNRAS* ([arXiv:1501.03212](https://arxiv.org/abs/1501.03212)),
- Salvadori S., Skuladottir A., Tolstoy E., 2015, accepted to *MNRAS* ([arXiv:1506.03451](https://arxiv.org/abs/1506.03451)),
- Sasaki M., Clark P. C., Springel V., Klessen R. S., Glover S. C. O., 2014, *MNRAS*, 442, 1942
- Schneider R., Omukai K., Bianchi S., Valiante R., 2012, *MNRAS*, 419, 1566
- Shu F. H., Lizano S., Galli D., Cantó J., Laughlin G., 2002, *ApJ*, 580, 969
- Sluder A., Ritter J., Safrank-Shrader C., Milosavljevic M., Bromm V., 2015, *MNRAS*, submitted ([arXiv:1505.07126](https://arxiv.org/abs/1505.07126)),
- Smith B., Wise J., O'Shea B., Norman M., Khochfar S., 2015, *MNRAS*, 452, 2822
- Stacy A., Greif T. H., Bromm V., 2010, *MNRAS*, 403, 45
- Stacy A., Greif T. H., Bromm V., 2012, *MNRAS*, 422, 290
- Susa H., Hasegawa K., Tominaga N., 2014, *ApJ*, 792, 32
- Sutherland R. S., Dopita M. A., 1993, *ApJS*, 88, 253
- Tegmark M., Silk J., Rees M. J., Blanchard A., Abel T., Palla F., 1997, *ApJ*, 474, 1
- Tinsley B. M., 1980, *Fundamentals Cosmic Phys.*, 5, 287
- Tominaga N., Umeda H., Nomoto K., 2007, *ApJ*, 660, 516
- Tominaga N., Iwamoto N., Nomoto K., 2014, *ApJ*, 785, 98
- Tumlinson J., 2006, *ApJ*, 641, 1
- Umeda H., Nomoto K., 2002, *ApJ*, 565, 385
- Umeda H., Nomoto K., 2003, *Nature*, 422, 871
- Vargas L. C., Geha M., Kirby E. N., Simon J. D., 2013, *ApJ*, 767, 134
- Vargas L. C., Geha M. C., Tollerud E. J., 2014, *ApJ*, 790, 73
- Wada K., Venkatesan A., 2003, *ApJ*, 591, 38
- Wang F. Y., Bromm V., Greif T. H., Stacy A., Dai Z. G., Loeb A., Cheng K. S., 2012, *ApJ*, 760, 27
- Webster D., Sutherland R., Bland-Hawthorn J., 2014, *ApJ*, 796, 11
- Whalen D., van Veelen B., O'Shea B. W., Norman M. L., 2008, *ApJ*, 682, 49
- Whalen D. J., Fryer C. L., Holz D. E., Heger A., Woosley S. E., Stiavelli M., Even W., Frey L. H., 2013, *ApJ*, 762, L6
- Wise J. H., Abel T., 2007, *ApJ*, 665, 899
- Wise J. H., Turk M. J., Norman M. L., Abel T., 2012, *ApJ*, 745, 50
- Yoshida N., Omukai K., Hernquist L., Abel T., 2006, *ApJ*, 652, 6
- de Souza R. S., Ishida E. E. O., Whalen D. J., Johnson J. L., Ferrara A., 2014, *MNRAS*, 442, 1640